Chem Soc Rev

TUTORIAL REVIEW

View Article Online
View Journal | View Issue

Cite this: *Chem. Soc. Rev.*, 2025, **54**, 11468

Ab initio electronic structure calculations of lanthanide single-molecule magnets; a practical guide

Nicholas F. Chilton [ab]

Received 4th September 2025

DOI: 10.1039/d5cs00493d

rsc.li/chem-soc-rev

Research into single-molecule magnetism lies at the nexus of challenging synthetic chemistry, spin physics and *ab initio* quantum chemistry. There are no "one-size-fits-all" textbooks and as such it can be challenging for beginners to navigate the intersection of these fields. This tutorial review is intended as a primer for preparation and interpretation of *ab initio* calculations of lanthanide single-molecule magnets, with a specific focus on using the OpenMolcas program.

Key learning points
(1) The spin Hamiltonian formalism.
(2) Connection between quantum states and ensemble measurements.
(3) Basics of *ab initio* multiconfigurational quantum chemistry.
(4) Basic principles of single-molecule magnetism.
(5) Tangible understanding of magnetic anisotropy.

[a] *Research School of Chemistry, The Australian National University, Acton 2601, Australia. E-mail: nicholas.chilton@anu.edu.au*
[b] *Department of Chemistry, The University of Manchester, Manchester M13 9PL, UK*

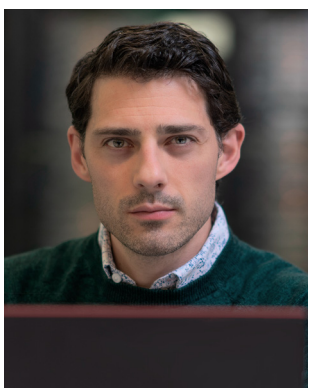

Nicholas F. Chilton

Nicholas F. Chilton is a Professor of Chemistry at The Australian National University, and a Professor of Computational and Theoretical Chemistry at The University of Manchester. He obtained his BSc Adv Hons at Monash University in 2011, under the supervision of Prof. Keith Murray, and his PhD from The University of Manchester in 2015 under the supervision of Prof. Richard Winpenny and Prof. Eric McInnes. He was previously a Ramsay Memorial Fellow, a University of Manchester Presidential Fellow, and a Royal Society University Research Fellow. He is a fellow of the Royal Society of Chemistry and the Royal Australian Chemical Institute.

1 Introduction

Single-molecule magnets[1–5] are a class of coordination complexes where the ligands impart a crystal field potential such that the ground magnetic states of the ion(s) experience an easy-axis magnetic anisotropy. The presence of magnetic anisotropy is equivalent to stating that different projections of the total angular momentum (this could be spin, S, where the projections are m_S or S_z, or spin plus orbit, J, where the projections are m_J or J_z) have different energies. When the anisotropy is easy-axis type, the projections of the total angular momentum along one direction are energetically favoured, compared to those in the plane perpendicular to it (the so-called hard plane). For example, if the total angular momentum is $J = 15/2$ (such as Dy^{III}, the most common metal ion employed for modern SMMs), then the $m_J = \pm 15/2$ states which have the largest projections along the quantisation axis (often synonymised with the z-axis, hence the subscripts S_z or J_z; we will return to this point in detail later) are stabilised compared to the $m_J = \pm 1/2$ states which have the smallest projections along the quantisation axis. The physical interpretation is that if the total angular momentum vector $\vec{J}$ points as close to "up" or "down" the energy is minimised compared to when $\vec{J}$ points close to the perpendicular plane (Fig. 1, for $J = 3/2$). If all the

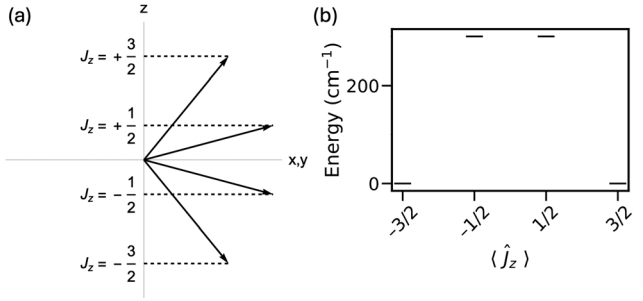

Fig. 1 (a) Quantised projections of a total angular momentum $J = 3/2$. (b) Energies of the projections of the total angular momentum for an easy-axis magnetic anisotropy.

states in between "up/down" and "in-plane" (recall that $m_J = -J, -J + 1, \ldots, J - 1, J$) smoothly vary in energy, then we can associate the easy-axis magnetic anisotropy with an energy barrier to re-orientation of the magnetic moment (Fig. 1b), referred to as U_{eff}. [As an aside, recall that the total angular momentum vector $\vec{J}$ (or equally $\vec{S}$) cannot point directly along the quantisation axis, as its length $\sqrt{J(J+1)}$ is greater than its largest projection on that axis $m_J = J$.] When the energy barrier is larger than the thermal energy available to the molecule, *i.e. via* vibrational energy, the magnetic moment cannot freely reverse its direction. This leads to a magnetic memory effect that depends on temperature and timescale, and hence, the origin of a SMM.

The practicalities of designing SMMs and measuring their properties have been expounded in various other texts[2,6–11] and we will not dwell on these matters here. Rather, this article is intended as guide for connecting *ab initio* quantum chemical calculations (the pioneering work of Chibotaru and Ungur for popularising *ab initio* calculations on SMMs is recommended reading,[12–15] particularly their book chapter[16]) to spin Hamiltonian models and to experimental interpretation. We will focus on use and interpretation of CASSCF-SO using OpenMolcas,[17–20] however the guidance herein can be equally taken for use with Orca,[21] or any other CASSCF software package with the required functionality.

Research in the field of molecular magnetism tends to accumulate numerous minutiae that are assumed knowledge that seem to cross discipline boundaries, making study of this area difficult without significant experience or a knowledgeable guide. In this article I have tried to impart my experience to serve as a reference for newcomers. Throughout we will focus on the case of Dy^{III}, being the most emblematic of ions associated with SMMs besides Mn^{III},[5,22] but the discussions are equally relevant to the electronic structure of any other Ln^{III} ion, and with some modifications can be generalised to d-block or 5f ions.

2 Electronic structure of trivalent 4f ions

We begin with a brief recap of the electronic structure of Ln^{III} ions.[23,24] The 4f (5f) orbitals are unique in the periodic table, in that they are filled after the more radially-extensive 6s, 5s and 5p orbitals (7s, 6s and 6p), the latter two of which remain fully-occupied in the trivalent ions (*i.e.* the Ln^{III} ions have $4f^n5s^25p^6$ configurations). Hence, in complexes of the Ln^{III} ions, the 4f orbitals are well-shielded from the environment and are essentially non-bonding (we will see later that even in complexes the 4f orbitals are roughly 99.9% pure atomic 4f orbitals).

In the presence of a degenerate set of orbitals, excluding the half-filled $4f^7$ case of Gd^{III}, we are free to choose from many different electronic occupations which on paper all have the same energy. This is the so-called "orbital degeneracy" that gives rise to an orbital angular momentum, an additional source of magnetism on top of the spin angular momentum of the unpaired electrons. In a classical analogy, the freedom of electrons to hop between 4f orbitals with no energy penalty can be thought of as a "current" around the atom, which gives rise to its own magnetic field. Under this classical analogy, it should be no surprise that two magnetic moments (spin and orbital momenta) will interact with each other: this is the spin–orbit coupling. Note, however, that spin–orbit coupling is actually a relativistic effect which arises due to the confluence of special relativity and quantum mechanics (see the Dirac equation), and so the classical analogy can only go so far.

Nonetheless, the spin–orbit coupling does as its name suggests: the spin and orbital momenta (quantum numbers S and L, respectively) are coupled into a total angular momentum (quantum number J). Note that the spin and orbital angular momenta are vector quantities, and so the summation to make the total angular momentum (*i.e.* $\vec{J} = \vec{L} + \vec{S}$) follows vector addition rules, leading to allowed quantum numbers $J = |L - S|, |L - S| + 1, \ldots, L + S - 1, L + S$.

For the simplest Ln^{III} ions Ce^{III} and Yb^{III} (which have $4f^1$ and $4f^{13}$ configurations, respectively), the spin quantum number is $S = 1/2$ and the orbital angular momentum quantum number is $L = 3$. A pair of definite spin and orbital quantum numbers defines a Russell–Saunders (RS) or LS term and is given in spectroscopic notation ^{2S+1}L (recalling that spin multiplicity is given by $2S + 1$ and that $L = 0 \rightarrow S$, $L = 1 \rightarrow P$, $L = 2 \rightarrow D$, *etc.*) and hence for both Ce^{III} and Yb^{III}, the RS electronic term is ^{2}F. After spin–orbit coupling, this term gives rise to $J = 5/2$ and $J = 7/2$, which are each referred to as spin–orbit multiplets, and given as $^{2S+1}L_J$. Hence, for Ce^{III} and Yb^{III} we have the $^2F_{5/2}$ and $^2F_{7/2}$ multiplets. Determination of which spin–orbit multiplet is lowest in energy is dictated by the number of 4f electrons: for <7 4f electrons the smallest J multiplet is the ground state, while for >7 4f electrons the largest J multiplet is the ground state. As it is the spin–orbit coupling that breaks the $(2S + 1)\times(2L + 1)$ degeneracy of the RS terms, the energy separation between J multiplets is related to the spin–orbit coupling constant. Spin–orbit coupling increases across the 4f series from $\zeta = 640$ cm^{-1} for Ce^{III} ($Z = 58$) to $\zeta = 2950$ cm^{-1} for Yb^{III} ($Z = 70$),[25] with an approximately quadratic dependence on Z.[26–28] The 4f spin–orbit coupling constant ζ is often transformed into the relative spin–orbit coupling constant λ for a given RS term, with the relation $\lambda = \pm\zeta/2S$, where the + sign is for <7 4f electrons and the $-$ sign for >7 4f electrons.

For other Ln^{III} ions with more than one unpaired electron, there are far more RS terms. The ground RS term is dictated by Hund's rules, which specify that the term with largest spin, and then largest orbital angular momentum, is lowest in energy. For Dy^{III}, the ground Hund's rule RS term is ^6H, with $S = 5/2$ and $L = 5$. After spin–orbit coupling we have $J = 5/2$, 7/2, 9/2, 11/2, 13/2, 15/2, and as Dy^{III} is $4f^9$ the $^6H_{15/2}$ multiplet is the ground state and the $^6H_{13/2}$ multiplet lies at approximately 3500 cm^{-1} (Fig. S1).[29]

The J multiplets contain $2J + 1$ m_J states each, which for a free ion (*i.e.* gas-phase Ln^{III}) are all degenerate. Once a Ln^{III} ion is incorporated into a complex or material, the removal of spherical symmetry removes the $2J + 1$ degeneracy of the m_J states, which is usually termed the crystal field or ligand field splitting; we will return to this in some detail. For achieving good SMM performance, one wishes to have a large magnetic moment, and thus maximising J is wise. Hence, the later 4f ions, Tb^{III}, Dy^{III}, Ho^{III} and Er^{III} have attracted the most attention.

The final consideration on choice of Ln^{III} ion is the spin parity. Ions with an odd number of unpaired electrons are subject to a time-reversal symmetry, also known as Kramers theorem, which means that in the absence of a magnetic field all electronic states must be at least doubly-degenerate. This guarantees that for any such ion (a Kramers ion), no matter the shape of molecule, the ground state will always be magnetic and have the possibility of supporting a magnetic memory effect. This is not the case for ions with even numbers of unpaired electrons (non-Kramers ions), which can have singlet ground states that are intrinsically non-magnetic in small magnetic fields. Hence, the most common Ln^{III} ions for SMMs are the Kramers ions Dy^{III} and Er^{III}.

3 Hamiltonian matrices and diagonalisation

Before we can discuss SMM-specific details, we need to briefly recap how we solve quantum mechanical models using linear algebra techniques. Whether we are talking about a quantum chemical calculation or a spin Hamiltonian model, both approaches share common elements. Those are: (i) definition of a Hamiltonian operator $\hat{H}$, (ii) choice of basis, (iii) calculation of matrix elements for the matrix representation of the Hamiltonian operator $\overline{\overline{\hat{H}}}$, and (iv) diagonalisation of $\overline{\overline{\hat{H}}}$ to determine the wavefunctions (eigenvectors) and energies (eigenvalues). When we construct the matrix representation of an operator, including the Hamiltonian, we usually do this using a complete and orthonormal basis set, which defines the Hilbert space. We associate the solution to the Hamiltonian as the set of eigenvalues and eigenvectors that diagonalise its matrix representation. A crucial concept is that the set of eigenvectors are a mutually-orthogonal set that spans the same Hilbert space, such that matrix diagonalisation can be viewed as a rotation in the Hilbert space. In linear algebra terms, the set of eigenvectors expressed as column vectors and packed into a matrix form (here given the symbol $\overline{\overline{\Psi}}$) is a unitary matrix that performs the rotation:

$$\overline{\overline{\Psi}}^{-1}\overline{\overline{\hat{H}}}\,\overline{\overline{\Psi}} = \overline{\overline{E}}$$

The matrix $\overline{\overline{E}}$ is a diagonal matrix that contains the eigenvalues on its diagonal, one for each eigenvector or eigenstate, which together are termed eigenpairs. The eigenvectors obtained from the matrix diagonalisation process are determined up to an arbitrary complex phase. That is, if $|\psi_k\rangle$ is an eigenvector of the Hamiltonian and hence $\overline{\overline{\hat{H}}}|\psi_k\rangle = E_k|\psi_k\rangle$, then $e^{i\varphi}|\psi_k\rangle$ is also an eigenvector with the same eigenvalue for any real φ, where i is the imaginary unit $i = \sqrt{-1}$.

As an explicit example, we will focus on the $J = 15/2$ problem connected with Dy^{III} SMMs. Throughout this work we will use a hypothetical model complex, $[Dy(OH)Br]^+$, purposely defined to be non-linear and using an odd choice of molecular coordinate frame, where the pertinent internal coordinates are: Br–Dy = 3.2 Å, Dy–O = 2.6 Å, O–H = 1.0 Å, Br–Dy–O = 175°, Dy–O–H = 110°. Later, we will interrogate the results of an explicit *ab initio* calculation on this molecule as an example, using OpenMolcas[17–20] and our molcas_suite and angmom_suite toolboxes.[30,31]

While later we will consider the full low-symmetry Hamiltonian, we start here by assuming that the axial magnetic anisotropy imposed by the near-linear disposition of bromide and hydroxide ligands can be simply modelled by the crystal field Hamiltonian $\hat{H} = B_2^0\theta_2\hat{O}_2^0$. We will not review the crystal field operator equivalent method here, and instead direct readers to references,[32–37] but suffice it to say that when considering crystal field splitting of a Ln^{III} ion in the in the $|J, m_J\rangle$ basis, the $\hat{O}_2^0$ operator is proportional to $\hat{J}_z^2$, so that for this example we will simplify our Hamiltonian to read $\hat{H} = A\hat{J}_z^2$. To proceed, we evaluate the matrix representation of the Hamiltonian by calculating the matrix elements of the Hamiltonian operator in the $|J = 15/2, m_J\rangle$ basis, usually referred to as the $|m_J\rangle$ basis, which canonically are assumed as eigenstates of the $\hat{J}_z$ operator; that is, $\hat{J}_z|m_J\rangle = m_J|m_J\rangle$. Hence, we can immediately determine the matrix elements to be:

$$\begin{aligned}\langle m_J'|\hat{H}|m_J\rangle &= \langle m_J'|A\hat{J}_z^2|m_J\rangle = \langle m_J'|Am_J\hat{J}_z|m_J\rangle \\ &= \langle m_J'|Am_J^2|m_J\rangle = Am_J^2\langle m_J'|m_J\rangle = Am_J^2\delta_{m_J',m_J}\end{aligned}$$

where $\delta_{k,n}$ is the Kronecker delta ($\delta_{k,n} = 1$ if $k = n$; $\delta_{k,n} = 0$ if $k \neq n$). This defines a diagonal matrix with Am_J^2 on the diagonal. Thus, we need not diagonalise the matrix: the $|m_J\rangle$ or $\hat{J}_z$ basis is already the eigenbasis for this Hamiltonian. Hence, we can read the energy values of each m_J state from the diagonal which are just Am_J^2. In the case of the $[Dy(OH)Br]^+$ molecule, we expect a $m_J = \pm 15/2$ ground state owing to the near-linear disposition of negative charges,[6,38,39] and so this molecule

would have $A < 0$ for a spin Hamiltonian model defined as $\hat{H} = A\hat{J}_z^2$.

Now consider the case where we decided that we should instead write our Hamiltonian as $\hat{H} = A\hat{J}_x^2$. Perhaps this is because we have defined our molecular geometry such that the main anisotropy axis is along the x-axis. We could of course just choose to write our Hamiltonian in an $|m_J\rangle$ basis that was instead defined as eigenstates of the $\hat{J}_x$ operator, and then we would obtain exactly the result as before. But for the sake of illustration, let's continue with the evaluation of the Hamiltonian in the canonical $\hat{J}_z$ eigenbasis. We start by defining the $\hat{J}_x$ operator in terms of the raising and lowering operators $\hat{J}_x = \frac{1}{2}(\hat{J}_+ + \hat{J}_-)$, and hence $\hat{J}_x^2 = \frac{1}{4}(\hat{J}_+^2 + \hat{J}_+\hat{J}_- + \hat{J}_-\hat{J}_+ + \hat{J}_-^2)$. Evaluation of the matrix elements is now more tedious, but is simple enough using the fundamental rules $\hat{J}_\pm|m_J\rangle = \sqrt{J(J+1) - m_J(m_J \pm 1)}|m_J \pm 1\rangle$. The working is:

$$\begin{aligned}
\langle m_J'|\hat{H}|m_J\rangle &= \left\langle m_J'\middle|\frac{A}{4}(\hat{J}_+^2 + \hat{J}_+\hat{J}_- + \hat{J}_-\hat{J}_+ + \hat{J}_-^2)\middle|m_J\right\rangle \\
&= \frac{A}{4}(\langle m_J'|\hat{J}_+^2|m_J\rangle + \langle m_J'|\hat{J}_+\hat{J}_-|m_J\rangle + \langle m_J'|\hat{J}_-\hat{J}_+|m_J\rangle + \langle m_J'|\hat{J}_-^2|m_J\rangle) \\
&= \frac{A}{4}\Big(\left\langle m_J'\middle|\sqrt{J(J+1) - (m_J+1)(m_J+2)}\sqrt{J(J+1) - m_J(m_J+1)}\middle|m_J+2\right\rangle \\
&+ \left\langle m_J'\middle|\sqrt{J(J+1) - (m_J-1)m_J}\sqrt{J(J+1) - m_J(m_J-1)}\middle|m_J\right\rangle \\
&+ \left\langle m_J'\middle|\sqrt{J(J+1) - (m_J+1)m_J}\sqrt{J(J+1) - m_J(m_J+1)}\middle|m_J\right\rangle \\
&+ \left\langle m_J'\middle|\sqrt{J(J+1) - (m_J-1)(m_J-2)}\sqrt{J(J+1) - m_J(m_J-1)}\middle|m_J-2\right\rangle\Big) \\
&= \frac{A}{4}\Big(\sqrt{J(J+1) - (m_J+1)(m_J+2)}\sqrt{J(J+1) - m_J(m_J+1)}\delta_{m_J',m_J+2} \\
&+ \left(2J(J+1) - 2m_J^2\right)\delta_{m_J',m_J} \\
&+ \sqrt{J(J+1) - (m_J-1)(m_J-2)}\sqrt{J(J+1) - m_J(m_J-1)}\delta_{m_J',m_J-2}\Big)
\end{aligned}$$

Clearly, this is no-longer a diagonal matrix as indicated by the Kronecker delta functions; still, out of the $16^2 = 256$ possible matrix elements, only 44 are non-zero. Note further that because any observable operator, including the Hamiltonian, must have a matrix representation that is Hermitian ($\overline{\overline{\hat{H}}} = \overline{\overline{\hat{H}}}^\dagger$, where the dagger operator is the conjugate-transpose), that only 22 matrix elements are unique. An alternative approach is to first evaluate the matrix representations of the $\hat{J}_+$ and $\hat{J}_-$ operators and then perform the appropriate matrix products and sum given in the first line of the above, *i.e.* the matrix representation of $\overline{\overline{\hat{J}_x^2}}$ can be determined from the sum $\overline{\overline{\hat{J}_x^2}} = \frac{A}{4}\left(\overline{\overline{\hat{J}_+^2}} + \overline{\overline{\hat{J}_+}}\,\overline{\overline{\hat{J}_-}} + \overline{\overline{\hat{J}_-}}\,\overline{\overline{\hat{J}_+}} + \overline{\overline{\hat{J}_-^2}}\right)$. Diagonalisation of $\overline{\overline{\hat{H}}}$ defined by $\hat{H} = A\hat{J}_x^2$ in the canonical $\hat{J}_z$ eigenbasis gives exactly the same result as before: a set of doubly-degenerate eigenvalues Am_J^2. However, the corresponding eigenvectors are obviously not the same $\hat{J}_z$ eigenfunctions, but linear combinations of them that serve to diagonalise the $\hat{J}_x^2$ operator. For instance, the ground $m_J = +15/2$ state when the uniaxial anisotropy is defined along the x-axis has the following representation in the $\hat{J}_z$ eigenbasis:

$$\begin{aligned}
\left|\psi_{+15/2}\right\rangle = \frac{1}{128\sqrt{2}}\Big(&|+15/2\rangle + \sqrt{15}|+13/2\rangle \\
&+ \sqrt{105}|+11/2\rangle + \sqrt{455}|+9/2\rangle \\
&+ \sqrt{1365}|+7/2\rangle + \sqrt{3003}|+5/2\rangle + \sqrt{5005}|+3/2\rangle \\
&+ \sqrt{6435}|+1/2\rangle + \sqrt{6435}|-1/2\rangle + \sqrt{5005}|-3/2\rangle \\
&+ \sqrt{3003}|-5/2\rangle + \sqrt{1365}|-7/2\rangle + \sqrt{455}|-9/2\rangle \\
&+ \sqrt{105}|-11/2\rangle + \sqrt{15}|-13/2\rangle + |-15/2\rangle\Big)
\end{aligned}$$

This compares to the eigenfunction of the ground $m_J = +15/2$ state for uniaxial anisotropy defined along the z-axis, and also written in the $\hat{J}_z$ eigenbasis, which is simply:

$$|\psi_{+15/2}\rangle = |+15/2\rangle$$

3.1 Consequences of Kramers theorem

We will not embark on a philosophical discussion of Kramers time-reversal theorem,[40] here we simply discuss how Kramers theorem is intrinsically linked to magnetism. This arises because the degeneracy of Kramers conjugate states is removed by time-odd operators such as the magnetic field; that is, an applied magnetic field removes the degeneracy (Fig. 2a). When this occurs, the relative population of the two states depends on the strength and direction of the magnetic field and hence a material with Kramers degeneracy in zero-magnetic field can be polarised by a magnetic field (Fig. 2a), which is the basis of

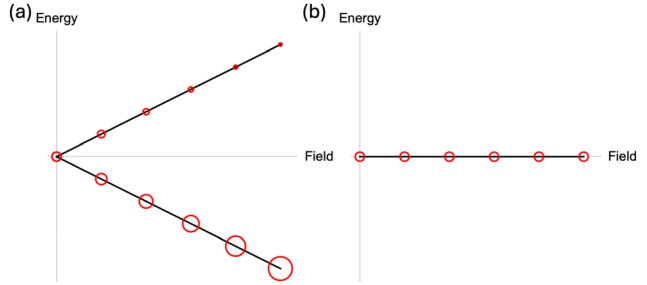

Fig. 2 Energies of a doublet state (a) and a singlet state (b) as a function of magnetic field with equilibrium populations represented by the radius of the red circles.

paramagnetism. Consider the opposite case where there are no degenerate states (*i.e.* all the states are singlets): as a small magnetic field is applied there is no change in energy, so that the population does not appreciably change, and hence there is no magnetic polarisation (Fig. 2b). For a large magnetic field, where the Zeeman Hamiltonian can dominate over other terms, there is a re-quantisation of the states towards eigenstates of the Zeeman Hamiltonian and as such singlet states can "bend" and take on non-zero magnetisation (see the Paschen–Back effect).

Returning to the case of Kramers degenerate states, we have several points to consider. In zero magnetic field we have degenerate eigenvalues, and from basic principles of linear algebra, degenerate eigenstates allow us to take arbitrary linear combinations of the two degenerate eigenvectors to define a new eigenvector in the degenerate subspace, where the second eigenvector is defined on the condition that the pair remain orthogonal. Returning to our J = 15/2 problem with Hamiltonian operator $\hat{H} = A\hat{J}_z^2$, we previously found that the m_J = ±15/2 eigenstates were degenerate with eigenvalue $A\left(\frac{15}{2}\right)^2$. In the J_z basis in which we most naturally construct this Hamiltonian, the eigenvectors are clearly $|{+15/2}\rangle$ and $|{-15/2}\rangle$. However, as the eigenvalues for these two eigenstates are degenerate, we can arbitrarily define two new eigenstates $|\psi_1\rangle = \frac{1}{\sqrt{2}}(|{+15/2}\rangle + |{-15/2}\rangle)$ and $|\psi_2\rangle = \frac{1}{\sqrt{2}}(|{+15/2}\rangle - |{-15/2}\rangle)$. We can prove these two states are orthogonal (where the simplification on the third line comes from the orthonormality of the basis states):

$$\begin{aligned}\langle\psi_1|\psi_2\rangle &= \frac{1}{\sqrt{2}}\left(\left\langle+\frac{15}{2}\right| + \left\langle-\frac{15}{2}\right|\right)\frac{1}{\sqrt{2}}\left(\left|+\frac{15}{2}\right\rangle - \left|-\frac{15}{2}\right\rangle\right)\\ &= \frac{1}{2}\left(\left\langle+\frac{15}{2}\right|+\frac{15}{2}\right\rangle - \left\langle+\frac{15}{2}\right|-\frac{15}{2}\right\rangle\\ &\quad + \left\langle-\frac{15}{2}\right|+\frac{15}{2}\right\rangle - \left\langle-\frac{15}{2}\right|-\frac{15}{2}\right\rangle\Big)\\ &= \frac{1}{2}(1-0+0-1) = 0\end{aligned}$$

and we can also prove that these two states share the same eigenvalue of $A\left(\frac{15}{2}\right)^2$:

$$\begin{aligned}\hat{H}|\psi_1\rangle &= A\hat{J}_z^2\frac{1}{\sqrt{2}}\left(\left|+\frac{15}{2}\right\rangle + \left|-\frac{15}{2}\right\rangle\right)\\ &= A\frac{1}{\sqrt{2}}\left(\left(\frac{15}{2}\right)^2\left|+\frac{15}{2}\right\rangle + \left(\frac{-15}{2}\right)^2\left|-\frac{15}{2}\right\rangle\right)\\ &= A\left(\frac{15}{2}\right)^2\frac{1}{\sqrt{2}}(|{+15/2}\rangle + |{-15/2}\rangle) = A\left(\frac{15}{2}\right)^2|\psi_1\rangle\end{aligned}$$

Hence, these states are equivalently eigenstates of the Hamiltonian $\hat{H} = A\hat{J}_z^2$. Thus, in general, any set of degenerate states can be rotated within the degenerate subspace and they remain eigenstates. Care must be taken in the case where states are more complicated linear combinations of the basis states, such that the rotation maintains the correct relative contributions of the different $|m_J\rangle$ functions. In any case, note that some arbitrary rotation means that these states are not eigenstates of $\hat{J}_z$, nor do they have to be, as they have only been defined as eigenstates of the Hamiltonian, $\hat{H} = A\hat{J}_z^2$ in this case. In practice, for ease of communication, it is conventional to choose the arbitrary linear combination such that the states are further eigenstates of some projection of the total angular momentum. This is usually achieved by applying a small magnetic field, because the Zeeman Hamiltonian is linear in the projection operators of the total angular momentum, see later.

4 *Ab initio* multiconfigurational quantum chemistry methods

4.1 Setting up a calculation

When attempting to describe ions that possess low-lying excited states, or indeed degenerate electron configurations, we are unable to rely on the basic assumptions of Hartree–Fock (HF) or density-functional theory (DFT) which are both defined assuming that the ground-state wavefunction is a single Slater determinant. As a reminder, a Slater determinant is a particular configuration of electrons in a set of orbitals.[41] For example, consider molecular hydrogen H_2: the ground state configuration $\sigma^2\sigma^{*0}$ defines a single Slater determinant (Fig. 3a), while the excited configuration $\sigma^1\sigma^{*1}$ defines four possible Slater determinants (Fig. 3b); the two determinants with parallel electron spins are the $m_S = \pm1$ states of the first excited S = 1 state, while the symmetric linear combination of spin up/down down/up corresponds to the m_S = 0 state of the first excited S = 1 state, and the antisymmetric linear combination of spin up/down down/up corresponds to the m_S = 0 state of the first excited S = 0 state. As an example for a Ln^{III} ion, consider Ce^{III} with a $4f^1$ configuration (Fig. 3c): the seven different choices of orbital and the two possible spin projections give 2 × 7 = 14 possible Slater determinants. This makes it obvious that if we would like to capture the electronic states of Ln^{III}, then we must incorporate more than one Slater determinant.

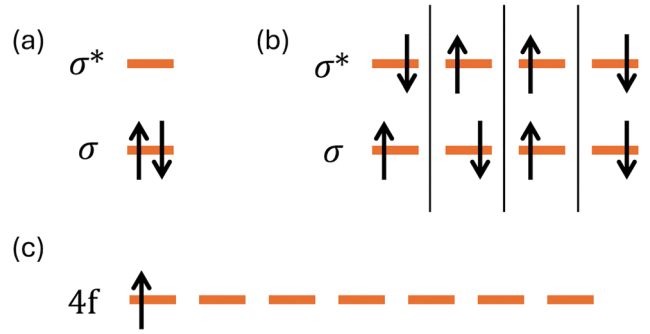

Fig. 3 Ground state (a) and excited state (b) Slater determinants for molecular hydrogen. One possible Slater determinant for the ground configuration of Ce^{III} (c).

This can be achieved with various multiconfigurational methods, but the most common in the context of SMMs is the complete active space self-consistent field (CASSCF) method.[42] This is because CASSCF is well-suited to cases with localised electron correlation such as atomic-like degeneracy, perfect to describe molecular Ln^{III} complexes. We can view the CASSCF method as an extension of HF theory, where we define the wavefunction as a linear combination of Slater determinants that are generated from a selected set of orbitals and electrons comprising the active space. For Ln^{III} ions, the minimal active space is the set of seven 4f orbitals (which are near-degenerate) and the n electrons that reside therein; this would be described as an "n in 7 active space", or a "(n,7) active space", or a "CAS(n,7)SCF calculation". Most CASSCF methods do not in fact use a basis of Slater determinants (which are individually eigenfunctions of the projection of the total spin, $m_S = \sum_k m_{s_k}$, where m_{s_k} is the spin projection of electron k), but rather use a basis of configuration state functions (CSFs) which are linear combinations of Slater determinants that are eigenstates of the total spin operator $\hat{S}^2$. This is chosen because then calculations can be performed using a scalar relativistic Hamiltonian without reference to the spin degrees of freedom (*i.e.* a spin-free Hamiltonian[43]). In this approach, CASSCF calculations are conducted separately for different total spin states, using a set of CSFs that are appropriately defined from the Slater determinants for the requested total spin quantum number (where only the $m_S = S$ component is explicitly calculated). Considering the ground ($\sigma^2\sigma^{*0}$) and first-excited ($\sigma^1\sigma^{*1}$) configurations of molecular hydrogen (Fig. 3), a minimal CAS(2,2)SCF would allow us to define two singlet CSFs (ground and first excited $S = 0$ states) and one triplet CSF (first excited $S = 1$ state).

Considering Dy^{III} which has a $4f^9$ ground configuration, the ground Hund's rule term is ^6H which has a total spin $S = 5/2$, but there also exists excited terms with the same total spin, such as ^6F, which would be possible states in a CASSCF calculation of sextet multiplicity. But to account for excited terms with different spin, for instance ^4F or ^4I ($S = 3/2$), or ^2K ($S = 1/2$), *etc.*, we would need a different spin-free CASSCF calculation for each spin multiplicity. These RS terms are split from one-another owing to the electron–electron repulsion in the $4f^n$ configuration; if the reader is unfamiliar with this concept, I recommend Condon and Shortley,[41] Abragam and Bleaney,[24] and Wybourne[23] as foundational texts, in addition to the "Dieke diagram",[44] which is a constant fixture on my office wall (Fig. S1). [If the reader is of the d-block persuasion, I suggest the texts of Figgis and Hitchman,[45] Gerloch,[46] Griffiths,[47] Mabbs and Machin,[48] as well as Abragam and Bleaney.[24]]

Returning to a practical application of a minimal CAS(n,7)SCF calculation, once we have chosen a particular manifold of total spin S, we must determine the wavefunction. This has two parts: determination of (i) the molecular orbitals (in which our active space is defined), and (ii) the linear combination of CSFs that are the eigenstates of the configuration interaction (CI) problem. Just like in HF theory, we define MOs as linear combinations of atomic orbitals (LCAO) which are atom-centred basis functions:

$$\psi_j[\vec{r}] = \sum_{A,\mu} c_{uj}^A \phi_\mu^A \left[\vec{r} - \vec{R}_A\right]$$

Here, the spatial MO ψ_j which has some amplitude and sign as a function of position $\vec{r}$ in the molecule, is formed as the sum over all possible basis functions ϕ_μ^A for each atom A. Note here that the "atom-centred" part is included by referencing the argument of the basis function to the nuclear position of the atom to which it is assigned, $\vec{R}_A$. [We note here that as all MOs are expanded in the same atomic orbital basis, that even the minimal "n in 7 active space" for a Ln^{III} ion is perfectly capable of capturing covalent effects; that is, the 7 active orbitals need not be 100% 4f character, although we will see later that this is nearly true anyway, revealing the staggering lack of covalency of the 4f shell. However the active space may be systematically expanded to include other frontier orbitals if those configurations are suspected to be significantly involved in the electronic structure of the Ln^{III} ion.[49,50]]

To obtain the MO coefficients c_{uj}^A, they must be variationally optimised to minimise the energy of the Hamiltonian.[51,52] However, we must account for all possible electron occupations in the active space that satisfy the chosen spin multiplicity, *i.e.* solving the CI problem. This amounts to finding the linear combination of CSFs that are eigenstates of the multiconfigurational Hamiltonian, which we can find by matrix diagonalisation. Thus, for each step in the self-consistent optimisation of the MO coefficients, we also solve the CI problem in the active space, which provides us with the energies of the different states of a given spin multiplicity.

As we have a wavefunction that can describe multiple electron configurations, we can describe numerous states: which ones should we choose to optimise the MOs for? In the case of Ln^{III} ions where we care about more than one state, we usually perform a state-average CASSCF (SA-CASSCF) calculation. Given the near-atomic nature of the active space, and that the 4f orbitals are generally non-bonding, the state-average approximation is quite robust for Ln^{III} ions. Naturally, it is a far poorer approximation when considering an active space comprised of bonding and anti-bonding orbitals (a common problem class), where

various excited states could easily have more-optimal MO descriptions. However, the considerable pain that would come from building multi-state wavefunctions from sets of MOs that were unique for every state does not usually justify the improved accuracy, notwithstanding numerical instabilities that can arise when attempting to variationally optimise excited state-specific MOs. The SA orbitals are thus a compromise for the set of states being considered.

Returning to SA-CASSCF, how many states, or roots of the characteristic polynomial defining the eigenstates of the Hamiltonian, do we choose? In the case of redox-innocent Ln^{III} ions, the choice is directly indicated by the Dieke diagram (Fig. S1, and because the 4f orbitals are core-like, this diagram is valid for nearly any coordination complex or solid-state material you could think of). Let's return to the case of Dy^{III}: our CAS(9,7)SCF calculation defines three possible total spin states, $S = 5/2$, $S = 3/2$ and $S = 1/2$ corresponding to multiplicities of 6, 4 and 2, respectively. First considering just the $S = 5/2$ states, for a 9 in 7 active space there are only 21 CSFs: these correspond to the ^{6}H, ^{6}F and ^{6}P RS terms in the Dieke diagram. Recall that by working with a spin-free scalar relativistic Hamiltonian using a basis of CSFs that are eigenstates of the total spin operator, we no-longer need to consider the spin degeneracy, and so we now only need to consider the multiplicity of the orbital angular momentum. The rules for determining the multiplicity of orbital angular momenta follow the same rules for any other angular momentum: the orbital multiplicity is simply $2L + 1$. Hence, for the ^{6}H term we have $L = 5$ giving $2L + 1 = 11$ states, for the ^{6}F term we have $L = 3$ giving $2L + 1 = 7$ states, and for the ^{6}P term we have $L = 1$ giving $2L + 1 = 3$ states; the sum of these multiplicities is $11 + 7 + 3 = 21$. It is no mistake that this matches the maximum dimension of the CSF basis defined by the choice of sextet spin multiplicity with a $4f^9$ active space: when considering well-defined ''atomic-like'' states, the multiplicity of the orbital angular momentum states span the space of CSFs for a given minimal active space when restricted to a particular total spin.

This knowledge also allows us to define the minimum number of states to include: a CAS(9,7)SCF calculation for a Dy^{III} complex considering the $S = 5/2$ states should account for at least 11 states (*i.e.* the whole ^{6}H term); other good choices would be 18 states (the ^{6}H and ^{6}F terms), or the full 21 states (the ^{6}H, ^{6}F and ^{6}P terms). It would be foolish to run calculations with a CAS(9,7)SCF wavefunction for a Dy^{III} complex for 1–10, 12–17, or 19–20 sextet roots: near-degenerate states within RS terms would be neglected, resulting in an incomplete L basis for a given term (*i.e.* some m_L states will be missing). Entirely analogous arguments can be made for states of different spin multiplicity for Dy^{III} and indeed for any other Ln^{III} ion. [These arguments must be adapted when considering d-block or 5f ions, depending on element, oxidation state and geometry. A good rule of thumb is to find large gaps in the spectra of the free-ion terms and omit things above a certain energy cut-off to avoid including very high-energy states that may not be required. However, perhaps these are required for a certain problem like optical absorption spectroscopy.]

Box 1.
In these boxes we will walk through an example SA-CASSCF-SO calculation for the $[Dy(OH)Br]^+$ molecule; the input and output files are in the associated data repository, and there is more detailed explanation in the SI. We have performed three SA-CASSCF calculations with a 9 in 7 active space: one for 21 sextets, one for 48 quartets, and one for 32 doublets. This corresponds to all possible sextet roots (^{6}H, ^{6}F and ^{6}P), but we have restricted the quartets to the lowest four terms (^{4}F, ^{4}I, ^{4}G and ^{4}M) and the doublets to the lowest two terms (^{2}L and ^{2}K).

4.2 Checking a CASSCF calculation

A crucial aspect of any CASSCF calculation is to check the orbitals to ensure that the active space is what you intended it to be. That is, if you ask for 9 active electrons in 7 active 4f orbitals, you best check that indeed you've converged a wavefunction that has this active space. This is because the self-consistent optimisation of thousands of MO and CI coefficients can converge into a local minimum that does not describe the electronic structure you intend, depending on the starting orbitals. The orbitals can be checked visually by rendering them, or by checking the MO coefficients themselves.

The second point is to consider the difference between the average orbitals and occupation numbers *versus* state-specific results. A SA-CASSCF calculation optimises one set of MOs in which you define the active space and hence the CSFs. The roots (eigenstates) are obtained by diagonalisation of the scalar relativistic Hamiltonian for a given set of MOs (this is the solution to the CI problem) and it is the average of the eigenvalues that is minimised by variational optimisation; in this case you can see how including lots of high-energy excited states can skew the quality of the SA-CASSCF wavefunction away from the ground states. With a converged SA-CASSCF wavefunction, the orbital occupation numbers tell you how the electrons occupy the MOs on average; for a well-behaved calculation on a Ln^{III} ion with a minimal active space we should obtain $n/7$ for all seven active orbitals (*e.g.* for Dy^{III} with 9 4f electrons we expect $9/7 \approx 1.29$) – if you do not obtain the expected number or they are not equal, something is not right! Aside from the average orbitals (also referred to as pseudo-natural orbitals), we may also obtain the natural orbitals for each root by diagonalisation of the one-electron density matrix:[53] we will not cover the theory here. The natural orbitals can be considered the state-specific spatial wavefunctions for the m_L states in each of the LS terms, noting that these are of little value for Ln^{III} ions because the spin–orbit coupling (SOC), which has yet to be included, is much larger than the crystal field splitting of the 4f orbitals which is relatively small. However, in cases where you are using more complicated active spaces and perhaps restricted active space (RAS) calculations,[54] the natural orbitals and their populations can provide useful information.[55]

Box 2.

After a SA-CAS(9,7)SCF calculation for the 21 sextets we examine the active space using our molcas_suite tool:

```
molcas_suite orbs 1.rasscf.h5 --index 2
```

We find:

```
---- MO 51, occ = 1.29, energy = -8.8063E-01, index = 2
  Dy1    4f     99.896
---- MO 52, occ = 1.29, energy = +1.3900E-08, index = 2
  Dy1    4f     99.978
---- MO 53, occ = 1.29, energy = +2.4105E-08, index = 2
  Dy1    4f     99.779
---- MO 54, occ = 1.29, energy = +1.0898E-06, index = 2
  Dy1    4f     99.973
---- MO 55, occ = 1.29, energy = -2.3893E-09, index = 2
  Dy1    4f     99.879
---- MO 56, occ = 1.29, energy = +4.8343E-07, index = 2
  Dy1    4f     99.920
---- MO 57, occ = 1.29, energy = -3.7632E-08, index = 2
  Dy1    4f     99.901
```

This indicates that the seven orbitals in the active space (index = 2) are well-described as 4f functions of Dy1. Visualisation of the active orbitals with Pegamoid[56] leads to the same conclusion:

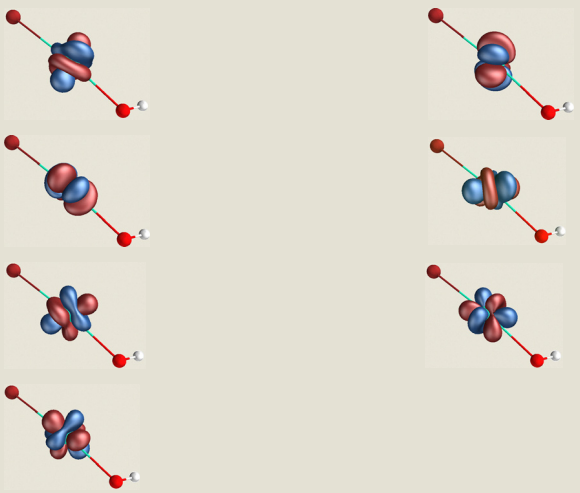

4.3 Inclusion of spin–orbit coupling

Usually for a Ln^{III} ion, we would perform a set of SA-CASSCF calculations to consider several spin multiplicities (using the approach above to determine how many states to include for each multiplicity). When these set of calculations are complete, the spin must be re-introduced and the effect of SOC must be included. This is generally referred to as a state-interaction approach where the SOC is included *a posteriori*. [Note that this means SOC is not included variationally – the MO and CI coefficients are not optimised considering SOC, but that this can be performed in some codes such as ORCA,[21] but indeed the state-interaction approach in OpenMolcas[57] is not a "perturbative treatment" of SOC either.] In this stage, the SOC Hamiltonian is formed in the spin-adapted basis of the various SA-CASSCF eigenstates. Then, as for any matrix representation of a Hamiltonian, the eigenstates are obtained by diagonalisation, giving the total SA-CASSCF spin–orbit (SA-CASSCF-SO) states, which will enumerate $\sum_i (2S_i + 1)n_i$ states in total where n_i are the numbers of roots for a given total spin S_i. At this stage, as it pertains to magnetism, we can obtain from the final SA-CASSCF-SO wavefunction: (i) the energies of the eigenstates, (ii) the matrix representations of the spin angular momentum in the eigenbasis of the SA-CASSCF-SO states (three matrices, $\hat{\vec{S}}_\alpha$, comprised of the matrix elements $\langle\psi_k|\hat{S}_\alpha|\psi_n\rangle$ where $\alpha \in x, y, z$ are the unit vectors of the

Box 3.

After obtaining the three SA-CASSCF wavefunctions, we calculate the SOC and determine the overall SA-CASSCF-SO eigenstates; here we have included all of the roots from our three SA-CASSCF calculations. The low-lying SA-CASSCF-SO spectrum shows:

SO State	D:o, cm**(-1)
1	0.0000
2	0.0000
3	546.3529
4	546.3529
5	1035.8587
6	1035.8587
7	1433.7079
8	1433.7079
9	1718.0046
10	1718.0046
11	1891.1705
12	1891.1705
13	1982.6057
14	1982.6057
15	2075.9211
16	2075.9211
17	3851.6439
18	3851.6439
19	4269.9149
20	4269.9149
21	4607.6792
22	4607.6792
23	4900.9881
24	4900.9881
25	5146.4215
26	5146.4215
27	5311.2641
28	5311.2641
29	5431.3921
30	5431.3921
31	6706.2338
32	6706.2338

As expected, we have pairs of degenerate states (Kramers doublets) and find 16 low-lying states (<2100 cm^{-1}), with the next 14 states between 3800 and 5500 cm^{-1}; the next states are >6700 cm^{-1}. I note that the gap between the barycentres (centre of gravity, average energy) of the multiplets is 3453 cm^{-1}, which is close to expected value of $\sim$3500 cm^{-1}. The SO splitting in SA-CASSCF-SO calculations is usually quite accurate, as the SOC Hamiltonian is built using an atomic approximation which is very good for the particular case of Ln^{III} complexes. The calculated energy gaps between adjacent terms (*e.g.* ^{6}H and ^{6}F) on the other hand are usually not so accurate because while these splittings arise from the 4f–4f electron repulsion (which is captured in SA-CASSCF), there are non-negligible effects arising from dynamic electron correlation with the other electrons in the molecule that are not captured. Hence, for accurate optical transition energies (*e.g.* the $^5D_0 \rightarrow {}^7F_0$ emission in Eu^{III} complexes), corrections for dynamic correlation in the form of CASPT2[58] or NEVPT2[59] are required.

orthogonal Cartesian reference frame defined by the input atomic coordinates), and (iii) the matrix representations of the orbital angular momentum in the eigenbasis of the SA-CASSCF-SO states ($\overline{\overline{\hat{L}}}_\alpha$, comprised of the matrix elements $\langle\psi_k|\hat{L}_\alpha|\psi_n\rangle$ where $\alpha \in x, y, z$).

Simply observing the spectrum of eigenvalues from the SA-CASSCF-SO calculation is an important step at this point. For the case of Dy^{III}, we should have 16 low-lying states (corresponding to the $^6H_{15/2}$ multiplet) split by the crystal field effect of the ligands, then, we should expect another tranche of 14 states (corresponding to the $^6H_{13/2}$ multiplet) around 3500 cm^{-1} higher in energy (refer to the Dieke diagram, Fig. S1). Keep in mind that at no point in the calculation have we explicitly told the quantum chemistry program that we have a $4f^9$ configuration and hence we should expect a $^6H_{15/2}$ ground multiplet. By virtue of selecting the MOs that correspond to the set of seven 4f orbitals as our active space, including 9 active electrons, requesting at least 11 sextet roots, and adding SOC, the resulting spectrum of eigenvalues should indeed match our expectations: this is the beauty of a fully-*ab initio* quantum chemical calculation. If our results do not comply with these expectations, however, that implies that something has gone wrong (or the chemistry is very interesting). In addition to checking the active space is as expected, this is an important part of verifying our work.

5 *Ab initio* magnetic properties

If we consider the eigenstates of the SA-CASSCF-SO calculation as those of the total zero-field Hamiltonian, we can calculate magnetic properties simply by adding the appropriate Zeeman term to the Hamiltonian, and diagonalising the resulting matrix. This is incredibly simple as we already have matrix representations of all these parts: the matrix representation of the SA-CASSCF-SO Hamiltonian in its eigenbasis is simply a diagonal matrix with the eigenvalues on the diagonal and zero elsewhere [*n.b.* this is nothing more than stating that $\hat{H}|\psi_k\rangle = E_k|\psi_k\rangle$], and the Zeeman Hamiltonian is $\overline{\overline{\hat{H}}}_{Zee} = \mu_B\left(\left(g_e\overline{\overline{\hat{S}}}_x + \overline{\overline{\hat{L}}}_x\right)B_x + \left(g_e\overline{\overline{\hat{S}}}_y + \overline{\overline{\hat{L}}}_y\right)B_y + \left(g_e\overline{\overline{\hat{S}}}_z + \overline{\overline{\hat{L}}}_z\right)B_z\right)$ where B_α are the components of the magnetic field, and μ_B and g_e are the Bohr magneton and free-electron gyromagnetic ratio, respectively. Once we have the eigenstates of the total Hamiltonian including magnetic field, thermodynamic properties such as magnetisation, magnetic susceptibility and heat capacity can be obtained from the properties of the eigenstates.[60–62] However, a note of caution is required here. Thermodynamic quantities calculated *ab initio* are obtained under three assumptions: (i) every molecule in the ensemble are identical to one-another, (ii) that there is no significant change in structure as a function of temperature, and (iii) that the ensemble is in thermodynamic equilibrium (that is, the population of the eigenstates are given by the Boltzmann distribution). It is crucial to keep in mind the limitations that these assumptions pose. For example, if there is disorder or dispersion in the molecular structure then the properties of the bulk may not be well-approximated by assuming all molecules are identical, in which case explicit distributions may be required.[63] If there are significant changes in structure as a function of temperature, then clearly this will need to be considered carefully on a case-by-case basis.[64,65] Finally, and perhaps most commonly, the assumption of equilibrium state populations for SMMs is often broken: this is a natural consequence of the slow-relaxation of magnetisation. A common consequence of this effect is the rapid decrease in $\chi_M T$ as a function of reducing temperature, often referred to as "magnetic blocking". As a paramagnet, the magnetic susceptibility of an SMM should follow the Curie law with $\chi_M \propto 1/T$ (hence $\chi_M T$ should be fairly constant). A gradual decrease in $\chi_M T$ on reducing temperature is expected as excited crystal field states are thermally depopulated, obeying Boltzmann statistics perfectly well. However, when the temperature is low enough that the relaxation dynamics are sufficiently slow, the magnetic susceptibility essentially becomes frozen on the timescale of the measurement, and is observed as a plateau. When plotted as the $\chi_M T$ product, the constant value of χ_M makes $\chi_M T$ appear as a linear function decreasing towards zero as T decreases towards zero.[66] Similar, but more complex, effects are observed during zero-field cooled *vs.* field cooled experiments that will be dependent on both the heating/cooling rates, the strength of the applied magnetic field and the details of the field and temperature dependent relaxation rates of the particular SMM.[8,67]

One property of the zero-field SA-CASSCF-SO eigenstates that is particularly useful in the case of Ln^{III} complexes is the effective *g*-values of the doublets. Just like the free-electron gyromagnetic ratio g_e, *g*-values describe the gradient of the energy levels in an applied magnetic field. In this case, they are termed "effective" *g*-values because these are not the "real" free-electron gyromagnetic ratio g_e. [Indeed, neither are they the Landé g_J-values that are defined for the Zeeman Hamiltonian written in the $|J, m_J\rangle$ basis $\hat{H}_{Zee} = \mu_B g_J(\hat{J}_x B_x + \hat{J}_y B_y + \hat{J}_z B_z)$, where $g_J = \frac{3}{2} - \frac{L(L+1) - S(S+1)}{2J(J+1)}$ under the approximation of $g_e = 2$.[24]] Under the action of the full *ab initio* SA-CASSCF-SO plus Zeeman Hamiltonian described above, the eigenstates will exhibit some magnetic field dependence, and the reader will note that indeed there is only one *g*-value included in the expression for $\overline{\overline{\hat{H}}}_{Zee}$ in the column to the left the "real" g_e. However, when we decide to look at a certain doublet independently of the others, we can define a model Hamiltonian in the two-dimensional space of an effective spin $S = 1/2$, also termed pseudo-spin or fictitious spin. The effective Zeeman Hamiltonian becomes:

$$\hat{H}_{Zee} = \mu_B(g_x\hat{S}_x B_x + g_y\hat{S}_y B_y + g_z\hat{S}_z B_z)$$

While the effective *g*-values above are often labelled g_x, g_y and g_z, these do not necessarily correspond to any lab or molecular frame; we will see later that such "principal" *g*-values are obtained by matrix diagonalisation and indeed the eigenvectors provide information on their spatial orientation. For pure m_J states we can determine the expected effective

Table 1 Effective principal g-values when treating pure m_J states of the J = 15/2 multiplet of Dy^{III} as pseudo-spin S = 1/2 states

m_J	g_x, g_y	g_z
±15/2	0	20
±13/2	0	52/3
±11/2	0	44/3
±9/2	0	12
±7/2	0	28/3
±5/2	0	20/3
±3/2	0	4
±1/2	32/3	4/3

g-values by simply equating the expectation value of the Zeeman Hamiltonian with a magnetic field along each of the Cartesian axis for a pseudo-spin doublet and the real m_J state. For the choice of the z-axis we obtain the following (considering only one component of each Kramers doublet):

$$\langle +1/2|\mu_B g_z \hat{S}_z B_z|+1/2\rangle = \langle m_J|\mu_B g_J \hat{J}_z B_z|m_J\rangle$$

$$\mu_B g_z B_z/2 = \mu_B g_J B_z m_J$$

$$g_z/2 = g_J m_J$$

$$g_z = 2 g_J m_J$$

For the x- and y-axes, the expectation values $\langle m_J|\mu_B g_J \hat{J}_\alpha B_\alpha|m_J\rangle$ (where $\alpha \in x, y, z$) are zero for all states, and hence $g_x = g_y = 0$. However for the $m_J = \pm 1/2$ states, the magnetic field mixes the two components in first-order, *i.e.* the off-diagonal elements are $\langle +1/2|\mu_B g_J \hat{J}_x B_x|\mp 1/2\rangle = 4\mu_B g_J B_x$ and $\langle \mp 1/2|\mu_B g_J \hat{J}_y B_y|\pm 1/2\rangle = \pm 4 i \mu_B g_J B_y$, and so we must diagonalise the two-dimensional subspace which gives eigenvalues of $\pm 4\mu_B g_J B_\alpha$ ($\alpha \in x, y$) in either case. A similar situation occurs for the off-diagonal elements of for spin S = 1/2, giving $\langle \mp 1/2|\mu_B g_x \hat{S}_x B_x|\pm 1/2\rangle = \mu_B g_x B_x/2$ and $\langle \mp 1/2|\mu_B g_y \hat{S}_y B_y|\pm 1/2\rangle = \pm i \mu_B g_y B_y/2$, which give eigenvalues of $\pm \mu_B g_\alpha B_\alpha/2$ ($\alpha \in x, y$). Thus, equating the eigenvalues of the Zeeman Hamiltonians for the $|J, \pm 1/2\rangle$ and $|S = 1/2, \pm 1/2\rangle$ subspaces we find $g_x = g_y = 8 g_J$ for the $m_J = \pm 1/2$ states. For Dy^{III} where g_J = 4/3, the resulting g-values are given in Table 1.

Generally speaking, this is just an application of perturbation theory in a particular subspace, and for Kramers doublets this treatment is natural; that is, they really do behave like S = 1/2 states with funny g-values (in the limit of a small magnetic field compared to the crystal field splitting between adjacent doublets). When the magnetic field is significant compared to the crystal field splitting, the doublets cannot be approximated as independent and the whole Hamiltonian must be considered. In this case, the Zeeman splitting can become non-linear when the magnetic field begins to dominate the Hamiltonian.

In the general case of a Kramers ion where we do not have pure m_J states, we can follow a simple procedure[68] to evaluate the action of the magnetic field *via* the Zeeman Hamiltonian in the two-dimensional subspace and define the effective g-values for the pseudo-spin S = 1/2 state. For various mathematical reasons, the three-by-three $\overline{\overline{g}}$ matrix to which we associate the magnetic properties of the pseudo-spin does not have the correct rotational properties to be considered a tensor,[24] which indeed means that it is not always symmetric or diagonalisable.[69] However, the three-by-three matrix GG^T is a well-behaved tensor and thus can always be diagonalised to yield principal effective g-values as the square root of its eigenvalues. Within the basis of a Kramers pair GG^T is defined as (where $\alpha, \beta \in x, y, z$ and k and n are the indices of the Kramers pair):

$$\begin{aligned}(GG^T)_{\alpha,\beta} = 2\Bigg(&\left(g_e\overline{\overline{\hat{S}}}_\alpha + \overline{\overline{\hat{L}}}_\alpha\right)_{k,n}\left(g_e\overline{\overline{\hat{S}}}_\beta + \overline{\overline{\hat{L}}}_\beta\right)_{n,k} \\ &+ \left(g_e\overline{\overline{\hat{S}}}_\alpha + \overline{\overline{\hat{L}}}_\alpha\right)_{n,k}\left(g_e\overline{\overline{\hat{S}}}_\beta + \overline{\overline{\hat{L}}}_\beta\right)_{k,n} \\ &+ \left(g_e\overline{\overline{\hat{S}}}_\alpha + \overline{\overline{\hat{L}}}_\alpha\right)_{n,n}\left(g_e\overline{\overline{\hat{S}}}_\beta + \overline{\overline{\hat{L}}}_\beta\right)_{n,n} \\ &+ \left(g_e\overline{\overline{\hat{S}}}_\alpha + \overline{\overline{\hat{L}}}_\alpha\right)_{k,k}\left(g_e\overline{\overline{\hat{S}}}_\beta + \overline{\overline{\hat{L}}}_\beta\right)_{k,k}\Bigg)\end{aligned}$$

Along with the eigenvalues, the eigenvectors provide the spatial orientation of the principal effective g-values in the coordinate system of the molecular structure. Note that in low-symmetry, there is no requirement for any of the doublets to share principal axes of their effective g-values; we will return to this later. Also note that this method gives no information on the sign of the effective g-values: the positive square root is taken by convention, but indeed g-values can be negative.[24,70,71]

The preceding approach can be taken for any Ln^{III} ion under the assumption of pure m_J states. However, for non-Kramers ions, note that all m_J basis states are integers, and so while in certain high symmetries there are doubly-degenerate states of the same $|m_J|$, there is no $m_J = \pm 1/2$ doublet and rather a m_J = 0 singlet; clearly, we cannot treat the latter as a pseudo-spin S = 1/2 state. In the case of general non-Kramers systems without pure m_J states there is not always rigorous double-degeneracy when the spatial symmetry is low. Thus, the doublets or near-degenerate doublets are usually referred to as pseudo- or Ising-doublets, and when using the GG^T approach, only one effective g-value is defined, while the other two are exactly zero.

Box 4.

Examination of the ground Kramers doublet shows:

```
                 g_1     g_2     g_3
g_1: 19.9127 x  0.7219 -0.6920  0.6354
g_2:  0.0000 y -0.6196 -0.6463  0.7699
g_3:  0.0000 z  0.3083  0.3215  0.0595
```

The eigenvalues g_1 through g_3 (labelled arbitrarily) are listed in the left column, and their corresponding eigenvectors (with respect to the Cartesian coordinate system x, y, z in which the input atomic coordinates were defined) are the relatively-labelled columns in the matrix on the right. In this example, we observe the ground doublet has its largest g-value g_1 = 19.91 pointing along the vector $\vec{v_1}$ = (0.7219, −0.6196, 0.3083). Note that the origin for this vector is ill-defined: it is simply an eigenvector of the GG^T matrix, obtained by assessing the effect of magnetic fields along the Cartesian axes in the molecular reference

frame. In the case of SA-CASSCF-SO calculations on molecules with well-localised spin and orbital angular momentum such as monometallic Ln^{III} complexes, the origin is well-approximated as the nucleus of the metal ion. Note also that as the two other g-values are degenerate, then the associated eigenvectors are completely arbitrary linear combinations of each other and they merely define the plane in which the zero g-values lie. This set of g-values is easy-axis and Ising-like (there is axial symmetry and the g-values perpendicular to the axis, $g_\perp$, are zero), with g_1 approaching that expected for a pure $m_J = \pm 15/2$ state (Table 1), so it would be a good assumption that this state is well-described as $|\pm 15/2\rangle$ if we choose the quantisation of the total angular momentum to lie along the same vector $\vec{v_1}$. If we plot this vector on the molecular structure using the PyMolVis software[72] (scaled so that it can be visible, as the eigenvectors are unit length, and considering its origin as the Dy atom), it points along the average Br–Dy–O axis as expected (Cartesian axes: x (red), y (green), z (blue)). Note that although we have drawn one vector $\vec{v_1}$, this direction defines an axis, so that plotting $-\vec{v_1}$ (or both) provides the same information.

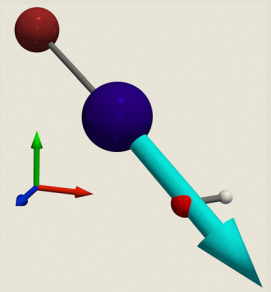

6 Orientations, reference frames and quantisation axes

Whenever we perform a quantum chemical calculation, the coordinate system or reference frame is defined by the input geometry. That is, we may define our $[Dy(OH)Br]^+$ complex in a sensible way with Dy at the origin and the bromine and oxygen atoms roughly along the z-axis, but of course this is completely arbitrary and the molecule could be in any orientation (as we have chosen for our example), and indeed it can be translated arbitrarily; the results of the calculation should not change depending on these choices. Thus, any result must be interpreted considering the reference frame defined by the molecular geometry. In the case of $[Dy(OH)Br]^+$ we expect an easy-axis magnetic anisotropy with a ground $m_J = \pm 15/2$ doublet along the Br–Dy–O axis. If we had defined the molecular geometry such that Br–Dy–O lay along the computational z-axis then we would find that one of the effective g-values approaching 20 would have an eigenvector approximately (0, 0, ±1). However, if the molecular geometry was defined with Br–Dy–O along the computational x-axis, the eigenvalue would still be the same value, but the eigenvector would be approximately (±1, 0, 0). This does not mean anything other than a permutation of the axes labels; after all, what does the computer know about up, down, left and right?

But what about if we don't know what the ordering or composition of the m_J states are, and we want to learn that from the calculation? This question can be answered in two ways: the first, purely *ab initio*, way is to calculate the expectation value of the total angular momentum along the quantisation axis. Conventionally, we refer to this as the z-axis, and hence we would like the expectation value of the $\hat{J}_z$ operator for each state, $\langle \hat{J}_z \rangle$. If we have made a fortuitous choice of molecular geometry such that the Br–Dy–O axis is parallel to the computational z-axis, then the expectation value $\langle \hat{J}_z \rangle = \langle \psi_i | \hat{J}_z | \psi_i \rangle = \langle \psi_i | \hat{L}_z | \psi_i \rangle + \langle \psi_i | \hat{S}_z | \psi_i \rangle \approx \pm 7.5$ for our ground $m_J = \pm 15/2$ doublet states (providing that the correct linear combination of the degenerate states is chosen to diagonalise $\hat{J}_z$). However, if we chose a less fortuitous orientation, say along the computational x-axis, then our calculation would give approximately $\langle \hat{J}_z \rangle \approx 0$. This is simply because our $m_J = \pm 15/2$ ground states would be nearly eigenstates of the $\hat{J}_x{}^2$ operator in our calculation (see above) not the $\hat{J}_z{}^2$ operator, so instead we would actually want to calculate $\langle \hat{J}_x \rangle$. Indeed, it usually makes more sense to re-label the axis system such that we follow convention with using the z-axis as the quantisation axis, which is just a rotation of the coordinate system. Once the choice of quantisation axis is made, we could calculate the $\langle \hat{J}_z \rangle$ expectation values for all doublets and attempt to assign m_J labels to the states, however this clearly would only work in the case of nearly pure $|m_J\rangle$ functions with no mixing, which is not a very general solution.

The second approach to answering this question is equivalent to asking how our *ab initio* Hamiltonian maps onto a model Hamiltonian constructed in a basis of definite angular momentum. There are many ways that this could be done, and the text herein is not exhaustive on the subject, nor will we cover many of the minutiae that must be considered in practical mapping codes.[73] In the simplest approach, where we have *a priori* knowledge of the expected electronic states (*e.g.* in the case of Ln^{III} complexes), we can take the first $(2J+1) \times (2J+1)$ sub-block of the *ab initio*-calculated $\overline{\overline{\hat{L}}}_z$ and $\overline{\overline{\hat{S}}}_z$ matrices (corresponding to the $2J+1$ states of the lowest J multiplet), and then form the matrix representation of $\hat{J}_z$ (*i.e.* $\overline{\overline{\hat{J}}}_z = \overline{\overline{\hat{S}}}_z + \overline{\overline{\hat{L}}}_z$). Note that these matrices are obtained from the calculation in the eigenbasis of the SA-CASSCF-SO calculation, and that from now on we assume that the z-axis is already defined as the quantisation axis of choice. Diagonalisation of $\overline{\overline{\hat{J}}}_z$ (which we assume is already in a basis that is diagonal in $\hat{J}^2$, *i.e.* we have chosen only one spin–orbit multiplet) gives eigenvalues of the $\hat{J}_z$ operator (which should be the values $m_J = -J, -J+1, \ldots, J-1, J$) as well as the unitary transformation matrix, $\overline{\overline{P}}_z$, that maps the *ab initio* SA-CASSCF-SO eigenstate basis to the $\hat{J}_z$ eigenstate basis (where $\overline{\overline{\hat{J}}}_{z,\mathrm{diag}-z}$ is a diagonal matrix containing the eigenvalues of $\overline{\overline{\hat{J}}}_z$):

$$\overline{\overline{P}}_z{}^{-1} \overline{\overline{\hat{J}}}_z \overline{\overline{P}}_z = \overline{\overline{\hat{J}}}_{z,\mathrm{diag}-z}$$

The square moduli of the matrix elements of $\overline{\overline{P}}_z$ tell us how much each $|m_J\rangle$ state (the rows as we go down each column) contributes to each SA-CASSCF-SO state (given by the columns). If we then use the unitary matrix $\overline{\overline{P}}_z$ to transform the $\overline{\overline{\hat{J}}}_x$ and $\overline{\overline{\hat{J}}}_y$

matrices (which are obtained similarly from the first $(2J+1)\times(2J+1)$ sub-block of the *ab initio*-calculated $\overline{\overline{\hat{L}}}_\alpha$ and $\overline{\overline{\hat{S}}}_\alpha$ matrices) in the same way, we can transform them into the $\hat{J}_z$ eigenstate basis. This works because they are all written initially in the same basis (the *ab initio* SA-CASSCF-SO eigenstate basis), so the same unitary transformation applied to all of them will put them all in the same basis.

$$\overline{\overline{P}}_z{}^{-1}\overline{\overline{\hat{J}}}_x\overline{\overline{P}}_z = \overline{\overline{\hat{J}}}_{x,\mathrm{diag}-z}$$

$$\overline{\overline{P}}_z{}^{-1}\overline{\overline{\hat{J}}}_y\overline{\overline{P}}_z = \overline{\overline{\hat{J}}}_{y,\mathrm{diag}-z}$$

By doing so $\overline{\overline{\hat{J}}}_{x,\mathrm{diag}-z}$ and $\overline{\overline{\hat{J}}}_{y,\mathrm{diag}-z}$ will not be diagonal matrices because the basis that diagonalises $\hat{J}_z$ does not also diagonalise $\hat{J}_x$ or $\hat{J}_y$ (this is just stating that we cannot have simultaneous eigenstates of $\hat{J}_x$, $\hat{J}_y$ and $\hat{J}_z$). However, because the eigenvectors of $\overline{\overline{\hat{J}}}_z$ (the columns of $\overline{\overline{P}}_z$) are only determined up to an arbitrary phase (see earlier), the $\overline{\overline{\hat{J}}}_{x,\mathrm{diag}-z}$ and $\overline{\overline{\hat{J}}}_{y,\mathrm{diag}-z}$ matrices will also not look like the canonically-expected matrix representations of $\hat{J}_x$ and $\hat{J}_y$. Hence, we must apply a phase factor to each column of $\overline{\overline{P}}_z$, such that the resulting $\overline{\overline{\hat{J}}}_{x,\mathrm{diag}-z}$ is purely real and positive, and $\overline{\overline{\hat{J}}}_{y,\mathrm{diag}-z}$ is purely imaginary (this is the Condon and Shortley choice of phase[41]), which results in the matrix $\overline{\overline{P}}_{z,\mathrm{phased}}$. We can then use this phase-adapted unitary transformation to transform the entire *ab initio* SA-CASSCF-SO Hamiltonian (which is simply a diagonal matrix with the energy eigenvalues as the diagonal elements, because it is given in its own eigenbasis) into the $\hat{J}_z$ basis which we will refer to as $\overline{\overline{\hat{H}}}_{\hat{J}_z}$:

$$\overline{\overline{P}}_{z,\mathrm{phased}}{}^{-1}\overline{\overline{E}}\,\overline{\overline{P}}_{z,\mathrm{phased}} = \overline{\overline{\hat{H}}}_{\hat{J}_z}$$

The $\overline{\overline{\hat{H}}}_{\hat{J}_z}$ matrix is now the SA-CASSCF-SO Hamiltonian in a definite basis of $\hat{J}_z$ eigenstates, with the correct phase behaviour of the canonical $\hat{J}_x$ and $\hat{J}_y$ operators. Hence, we can simply determine the matrix elements of a model Hamiltonian and directly equate the matrix elements to those of $\overline{\overline{\hat{H}}}_{\hat{J}_z}$ in the same positions and solve a set of linear equations to determine the parameters. For example, in the case of the $(2J+1)\times(2J+1)$ sub-block of the *ab initio* eigenstates for a Ln^{III} ion, we would usually like to know the coefficients corresponding to the crystal field splitting Hamiltonian written in terms of Stevens operators (where the θ_k are the operator equivalent factors that allow translation of the "true" B_k^q parameters into any basis, including the single electron f-orbital basis – they are tabulated for all ground multiplets and terms in the PHI user manual[62]):

$$\hat{H} = \sum_{k=2,4,6}\sum_{q=-k}^{k} B_k^q\theta_k\hat{O}_k^q$$

Here, at most we have 27 B_k^q parameters, and at least 36 matrix elements (for the smallest ground $J = 5/2$ of the Ln^{III} ions), and so the set of linear equations is over-determined, meaning that the solution is in-fact equivalent to a least-squares minimisation problem. Alternatively, we could use the fact that the $\hat{O}_k^q$ operators are related to the spherical harmonics and are a set of orthogonal operators in the angular momentum Hilbert space, and hence directly project the B_k^q parameters (exactly like a dot-product) without using a linear equation solver.[74,75] The approach we have just described is, roughly speaking, how the SINGLE_ANISO routine in OpenMolcas works.[76] Indeed, the above approach can also be performed in the spin-free basis using the first $(2L+1)\times(2L+1)$ sub-block orbital angular momentum $\overline{\overline{\hat{L}}}_{z,\text{spin-free}}$ which leads to definition of the crystal-field parameters in the $|L, m_L\rangle$ basis.

While this text is not intended as a tutorial on crystal field methods (see ref. 32–34 and 37), it is relevant here to point out that the restriction of the stevens operators to $k \in 2, 4, 6$ arises from the assumption that the crystal field is a real-one-electron operator acting on the 4f orbitals. As the angular part of single-electron atomic orbitals are defined by the spherical harmonics Y_l^m, and we can describe the effect of the crystal field also using spherical harmonics Y_k^q, this leads to integrals of the form:

$$\int_{\theta=0}^{\pi}\int_{\phi=0}^{2\pi} Y_l^{m'*}\,Y_k^q\,Y_l^m\sin\theta\,\mathrm{d}\theta\mathrm{d}\phi$$

Which are only non-zero if $k \le 2l$ and k is even, which leads to $k \in 2, 4, 6$ for f orbitals with $l = 3$. [Note that parameters with odd rank k arise when considering intra-configurational effects such as the crystal field mixing between d and f orbitals.[23,41]] However, if we consider the crystal field parameterisation to be purely phenomenological and not solely arising from this one-electron picture, then in principle the $\hat{O}_k^q$ operators have non-zero matrix elements for $k < 2J$ or $k < 2L$ depending on which basis is being used; however, as the one-electron crystal field effect is a good approximation for Ln^{III}, the terms $k > 6$ are usually quite small. Indeed, the $\hat{O}_k^q$ operators have a convenient property (because they are related to spherical harmonics Y_k^q) that they are a mutually-orthogonal set of operators. This means that every operator $\hat{O}_k^q$ will have a uniquely-defined B_k^q θ_k parameter when projecting them from $\overline{\overline{\hat{H}}}_{\hat{J}_z}$. Thus, in analogy to a Fourier transform, parameterisation of the full crystal field Hamiltonian (with all $k < 2J$ or $k < 2L$) provides an exact decomposition of the *ab initio* Hamiltonian into an orthogonal basis of operators.

With the crystal-field parameters in hand, they provide information on the contributions of the ligands to the Hamiltonian in a spherically-adapted basis. Hence, the $q = 0$ terms provide information on the axially-symmetric contributions, and the other terms with $q \neq 0$ provide information on the contributions related to C_q symmetry elements: *e.g.* terms with $q = 4$ are significant in square prismatic complexes that have pseudo C_4 rotation symmetry.[34,37] However, this would only be apparent if the quantisation axis for $\hat{J}_z$ was chosen to be coincident to the (pseudo) C_4 axis. As such, crystal field decompositions provide a route to interrogating the contributions of various symmetry

elements of the ligands to the total Hamiltonian, which can be used to rationalise magnetic and optical properties.[77,78] Finally, we note that the action of the operators $\hat{O}_k^q$ is to mix states with $\Delta m_J = \pm q$ so that for example a $\hat{O}_4{}^4$ term would mix the $|\pm 15/2\rangle$, $|\pm 7/2\rangle$, $|\mp 1/2\rangle$ and $|\mp 9/2\rangle$ states, *etc.*

In the case where there is no well-isolated manifold of states to directly assign to a chosen angular momentum, for instance the crystal-field splitting of a Dy^{III} ion was so large that the $J = 15/2$ and $J = 13/2$ manifolds overlapped, we need a different approach. Here, the alternative is one that uses projection operators to "extract" the angular momentum content from the *ab initio* eigenstates,[40,73,79] which is possible even if there is significant *J*-mixing. This is the approach that our "angmom_suite project" code takes.[31,73] Once this is done, the *ab initio* SA-CASSCF-SO Hamiltonian is transformed into the desired angular momentum basis (*e.g.* the $^6H_{15/2}$ multiplet or the entire ^6H term) and operators can be projected similarly to above. This approach is particularly useful for more complicated situations, including transition metals, $4f^n5d^m$ configurations, or molecules with more than one spin or orbital moment. In the latter cases we are able to separate the different contributions to the spin and orbital momenta and project a model Hamiltonian accounting for electron coupling; we will not discuss this here, but direct the reader to our recent works.[66,80–84]

For our $[Dy(OH)Br]^+$ example molecule, the obvious choice for the quantisation axis is along the average Br–Dy–O vector. But what about the far more common case where there is no clear choice? Usually in the case of SMMs we have designed molecules that support some kind of easy-axis magnetic anisotropy, following the classical electrostatic design rules for magnetic anisotropy in Ln^{III} complexes:[6,39] this would suggest two-coordinate linear for Dy^{III} and Tb^{III} and trigonal or square planar for Er^{III} (of course these perfect geometries are not obtained in practice). In such cases it is sensible to think about the pseudo-symmetry axis that appears somewhat unique compared to the plane perpendicular to it, even if this direction hosts no formal symmetry elements (*e.g.* along the average Cp_{cent}–Dy–Cp_{cent} vector in the case of dysprosocenium cations[85]). In cases where there is no such obvious choice, what should be done? Take for example the ubiquitous class of Ln^{III} tris beta diketonates – *e.g.* $[Ln(acac)_3(H_2O)_2]$,[86] $[Ln(acac)_3(phen)]$,[87] *etc.* – here, there is no clear axial direction, and yet, *ab initio* calculations for the Dy^{III} analogues of these two examples show that the ground state has $g_z > 19.5$ suggesting a $m_J = \pm 15/2$ state.[39] In these cases, choosing the quantisation axis as that defined by the eigenvector of the largest ground state *g*-value is sensible. It is common that once a quantisation axis is chosen that it is simply referred to as the *z*-axis.

Hence from our SA-CASSCF-SO calculations we can obtain $\langle \hat{J}_z \rangle$, and plotting these values *versus* energy for each state leads to the construction of the energy level diagram (Fig. 4a). [Note that usually a small magnetic field is applied along the *z*-axis so that the degeneracy of the states is completely removed and there is no ambiguity of arbitrary linear combinations, as discussed above.] In the case of $[Dy(OH)Br]^+$ we obtain something that looks just like we would expect for an SMM – an energy barrier between the ground $m_J = \pm 15/2$ states. However, if we had made a bad choice of the quantisation axis, say perpendicular to the average Br–Dy–O axis, then we would obtain something that does not look like an SMM (Fig. 4b). But how can this be?

Box 5.

Projection of the SA-CASSCF-SO Hamiltonian onto a crystal field model Hamiltonian for the $J = 15/2$ ground multiplet, defining the quantisation axis as the largest *g*-value of the ground Kramers doublet, using SINGLE_ANISO[76] gives:

k	q	B(k,q)
2	-2	-0.78605351390355E+00
2	-1	0.23116968488328E-02
2	0	-0.12304426032647E+02
2	1	0.41003797142487E-01
2	2	-0.12577057462565E+01
4	-4	0.21820207488647E-04
4	-3	0.18761027095137E-04
4	-2	-0.28588785122559E-03
4	-1	-0.40000233941737E-03
4	0	-0.38995029065723E-02
4	1	-0.23137016895326E-03
4	2	-0.48334928504280E-03
4	3	-0.27895807026883E-03
4	4	0.99021333988065E-05
6	-6	0.76612392124879E-09
6	-5	0.91000731757445E-08
6	-4	0.34079942295530E-08
6	-3	-0.88885824315653E-06
6	-2	0.11941157806199E-04
6	-1	0.83130004664506E-05
6	0	0.24141979675308E-04
6	1	-0.82510535529330E-06
6	2	0.18621636717687E-04
6	3	0.30477052552723E-05
6	4	0.11138285741133E-06
6	5	0.84318242117469E-07
6	6	0.53223222619884E-09

Note that these already include the operator equivalent factors θ_k for Dy^{III}, which for the $^6H_{15/2}$ multiplet are $\theta_2 = -2/315$, $\theta_4 = -8/135\,135$ and $\theta_6 = 4/3\,864\,861$, so these must be divided out to give the true B_k^q values (column one, Table S1). SINGLE_ANISO also gives the crystal field parameters in the $L = 5$ basis (column two, Table S1), which must similarly be divided by the appropriate operator equivalent factors for the ^6H term of Dy^{III}, which are $\theta_2 = -2/135$, $\theta_4 = -4/10\,395$ and $\theta_6 = 2/81\,081$; tables of the θ_k can be found in the PHI user manual.[62] The resulting parameters are slightly different owing their different method of extraction, but their similarity highlights the transferability of the Stevens operator equivalent method.[32]

We can also interrogate our resulting states without recourse to a model Hamiltonian using angmom_suite, which is particularly useful in cases when you are not sure of the angular momentum content:

```
angmom_suite proj --molcas_rassi DyBrOH.rassi.h5 \
                  > proj.out
```

Which gives information on the RS term content of the calculation (truncated for brevity):

```
Spin-free section:
S = 0.5
==================================
Term composition:
----------------------------------
1.02 |2K> = …
0.98 |2L> = …
…
S = 1.5
==================================
Term composition:
----------------------------------
1.00 |4F> = …
1.01 |4G> = …
1.03 |4I> = …
0.99 |4M> = …
…
S = 2.5
==================================
Term composition:
----------------------------------
0.99 |6P> = …
1.00 |6F> = …
1.00 |6H> = …
```

Showing that as expected we have the ^{2}K, ^{2}L, ^{4}F, ^{4}G, ^{4}I, ^{4}M, ^{6}P, ^{6}F and ^{6}H terms in the calculation. This can be useful for quantifying the mixing of $|L, m_L\rangle$ states or the orbital reduction owing to covalent effects (*i.e.* where L ceases to be a good quantum number). Then the spin–orbit states can be interrogated in the same way:

```
State composition:
----------------------------------
|State   1> (    0.00) = 0.95|6H15/2>
|State   2> (    0.00) = 0.95|6H15/2>
|State   3> (  546.35) = 0.93|6H15/2>
|State   4> (  546.35) = 0.93|6H15/2>
|State   5> ( 1035.86) = 0.93|6H15/2>
|State   6> ( 1035.86) = 0.93|6H15/2>
|State   7> ( 1433.71) = 0.93|6H15/2>
|State   8> ( 1433.71) = 0.93|6H15/2>
|State   9> ( 1718.00) = 0.93|6H15/2>
|State  10> ( 1718.00) = 0.93|6H15/2>
|State  11> ( 1891.17) = 0.94|6H15/2>
|State  12> ( 1891.17) = 0.94|6H15/2>
|State  13> ( 1982.61) = 0.94|6H15/2>
|State  14> ( 1982.61) = 0.94|6H15/2>
|State  15> ( 2075.92) = 0.94|6H15/2>
|State  16> ( 2075.92) = 0.94|6H15/2>
```

Showing that, as expected, the lowest 16 states correspond to the $^6H_{15/2}$ multiplet.

We can also use angmom_suite to project the parameters of a crystal field Hamiltonian for the $^6H_{15/2}$ multiplet using the lowest 16 states only. Note that here we have set the quantisation axis to be the direction of the maximal g-value of the ground Kramers doublet, using exactly the same choice of axes as SINGLE_ANISO above *via* the —quax keyword (column three, Table S1):

```
angmom_suite proj --molcas_rassi DyBrOH.rassi.h5 \
--model_space 6H15/2 --basis j --truncate 16 \
--terms cf=J --theta --ion Dy3+ --k_max 6 \
--quax quaxJ.txt --verbose > proj_152.out
```

This could also be done by projecting out all of the $^6H_{15/2}$ content from the wavefunction first, before projection (column four, Table S1):

```
angmom_suite proj --molcas_rassi DyBrOH.rassi.h5 \
--model_space 6H15/2 --terms cf=J --theta \
--ion Dy3+ --k_max 6 --quax quaxJ.txt --verbose \
> proj_6H152.out
```

Or in the $|L, S, m_S, m_S\rangle$ basis including the SOC Hamiltonian (again we've used the same quantisation axes as SINGLE_ANISO, however that code made a different choice in the $L = 5$ basis rather than the $J = 15/2$ basis, so that is reflected here for comparison; column five, Table S1):

```
angmom_suite proj --molcas_rassi DyBrOH.rassi.h5 \
--model_space 6H --terms cf=L soc=L,S --iso_soc \
--theta --ion Dy3+ --k_max 6 --quax quaxL.txt \
--verbose > proj_6H.out
```

From the projection in the $|L, S, m_S, m_S\rangle$ basis, we obtain the isotropic SOC value of $\lambda = -378$ cm^{-1}.

Building barrier figures like Fig. 4a is easy using the angmom_suite code (applying a 0.1 T field along the ground state anisotropy axis):

```
angmom_suite barrier --molcas_rassi DyBrOH.rassi.h5 \
--num_states 16 --save \
--Zeeman 0.07219 -0.06196 0.03083
```

6.1 Experiments are reality

The two most important experiments for quantification of SMM properties are measurement of the magnetic hysteresis and the relaxation rates by alternating current (AC) susceptometry.[2] In the former experiment, a large magnetic field is applied at low temperature to saturate the magnetic moment and then the magnetic field is swept to negative field and back to positive field again – the observation of a non-zero magnetic moment at zero field (the remanent magnetisation) is a key indicator of a magnetic memory effect.[2] In the latter experiment, an oscillating magnetic field is applied at low temperature and we measure the in-phase and out-of-phase response of the magnetic susceptibility.[2] Both experiments are usually performed on polycrystalline powders. Hence, there are some molecules that experience a magnetic field parallel to their easy axis, some that experience it in the hard plane, and for the other molecules the magnetic field is somewhere in between these limits. Considering the case of a perfect Ising-like easy-axis ground Kramers doublet ($g_x = g_y = 0$ and $g_z \neq 0$): a magnetic field along the easy-axis will lead to a splitting (Fig. 2a) while one in the hard-plane will lead to no splitting (Fig. 2b). Along the axis, we expect significant polarisation at low temperature according to Boltzmann statistics (of course the polarisation is smaller for an AC experiment which uses magnetic fields on the order of a few Oe (*ca.* 10^{-4} T) compared to the hysteresis experiment which usually uses fields on the order of a few T). [Note that the magnetic moment of a state is related to the gradient of its energy as a function of magnetic field $M_i \propto -\frac{dE_i}{dB}$, and the net magnetisation for an ensemble in equilibrium is simply the Boltzmann-weighted sum of the individual states' magnetic moments.] However, when the field is in the hard plane and the splitting is zero, there is no polarisation. For molecules in between, clearly it will be the projection of the magnetic field along their easy-axis that determines their magnetic polarisation. When the field is removed, only the molecules with a non-zero polarisation can contribute to the magnetisation or the

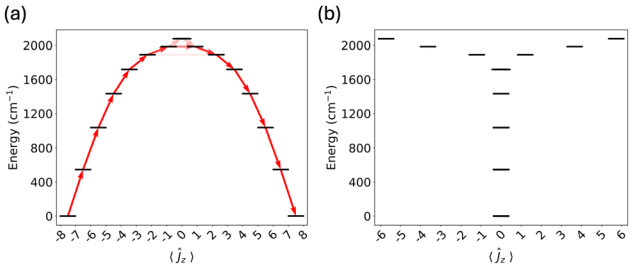

Fig. 4 Magnetic relaxation barrier for the choice of quantization axis along the Br–Dy–O axis (a) and perpendicular to the Br–Dy–O axis (b).

magnetic susceptibility. Hence, in the case of a perfect Ising magnetic material, the only relevant action of the magnetic field is how it impinges on the easy-axis of any of the molecules in the ensemble. Looking it another way, we care about how states are quantised and polarised by the applied magnetic field. Indeed, the choice of quantisation axis should be informed by the questions being asked in the experiment; and for SMMs, we care about magnetic fields along the easy-axis of the ground Kramers doublet.

In the general case of low-symmetry molecules that show some SMM effect (but do not have perfect Ising anisotropy), there is invariably an easy-axis anisotropy in the ground state where one effective *g*-value is larger than the other two which are considerably smaller. In these cases, the above interpretation is still a good approximation, and hence the direction of the largest effective *g*-value of the ground doublet is usually chosen as the quantisation axis to define J_z. In other cases where there is either easy-plane anisotropy (where two *g*-values of the ground doublet are larger than the third) or substantial rhombic anisotropy (where all three *g*-values are distinct), then the molecule will not be an SMM, and the quantisation axis in the former case is best chosen along the unique smallest *g*-value, while in the latter case there is no "good" choice and simply picking either the largest or smallest *g*-value is suitable. In any case, the quantisation axis used to perform these analyses must be stated. Hence, although the eigenstates behind both panels in Fig. 4 are the same, the choice of quantisation axis for Fig. 4b is "wrong" because measurement of the magnetisation dynamics will probe the properties of the molecule "looking" along the main magnetic axis of the ground state employed in Fig. 4a.

7 Energy barriers and quantum tunnelling of the magnetisation

So far we have quite extensively discussed the static properties of the ground multiplet, but this article is aimed at understanding slow magnetic dynamics and SMMs. We will not discuss the mechanisms of relaxation or the quantum tunnelling of the magnetisation (QTM) in detail; there is detailed literature on these more complex topics,[2,24,88–91] including a tutorial review recently published by our group on the former topic.[92] But we will discuss how the static properties of the calculated eigenstates can be connected with the experimental observation of slow relaxation in an AC susceptometry experiment. Several key concepts are required for a basic understanding of spin dynamics in SMMs:

(i) A molecule can only be in one quantum state at any time. However, we usually perform experiments on ensembles and so must consider the populations of a set of states, or the probability of a molecule being in one of those states.

(ii) If a molecule is in an eigenstate of the Hamiltonian it will remain in that state unless the Hamiltonian changes or it interacts with something outside the quantum system, *e.g.* with a phonon or photon.

(iii) Because magnetic moments are defined as $M_i \propto -\frac{dE_i}{dB}$ then any non-degenerate (singlet) state in zero magnetic field is non-magnetic; magnetic character can be switched on with an applied magnetic field when the states "bend".

The requirements for observation of SMM properties centre around the presence of an easy-axis anisotropy for a doubly-degenerate ground state;[7] hence, the first step is examination of the ground state.

7.1 Non-Kramers ions

Non-Kramers ions (with an even number of unpaired electrons) have integer total angular momentum *J* and the low-symmetry crystal field of a molecule can completely remove the degeneracy of the m_J states. That is, the ground state could be non-degenerate (a singlet ground state), for which there will be no SMM properties. However, even in the absence of symmetry, if there is sufficiently strong uniaxial magnetic anisotropy then the states can appear as pseudo-doublets. We refer to these as pseudo-doublets because in low symmetry there will be a small energy splitting between them. The splitting of the pseudo-doublets is referred to as the tunnelling gap or tunnel splitting and is directly related to the efficiency of zero-field QTM: $\tau_{QTM}^{-1} = 4(\Delta/\hbar)^2\tau_m$ where Δ is the tunnel gap and τ_m is related to the spin–phonon relaxation timescale.[93]

When a large magnetic field acts on a pseudo-doublet at low temperature, the pseudo-doublet will become polarised just like a Kramers doublet (Fig. 2a), and so for a large-enough field and/or low-enough temperature, the ensemble population will be near-unity in the lowest energy state (Fig. 5, red circle). If the magnetic field is reversed slowly enough then the Hamiltonian will change slowly (recall that inclusion of the Zeeman Hamiltonian will change the eigenstates as a function of magnetic field), and an individual molecule will remain in an eigenstate of the Hamiltonian at all times and simply follow the energy eigenvalue (Fig. 5, red arrow); this is called adiabatic passage. In this case, where there is a splitting of the pseudo-doublet in zero field, an avoided crossing is formed and adiabatic passage will lead to reversal of the magnetic moment because $\frac{dE_i}{dB}$ is negative on the right and positive on the left (Fig. 5, green circle): this is QTM.

If the magnetic field is reversed fast, then there is a non-zero probability that the molecule could remain on its trajectory and end up in the excited state (Fig. 5, blue circle) because it cannot change its eigenstate quick enough (Fig. 5, blue arrow); this is

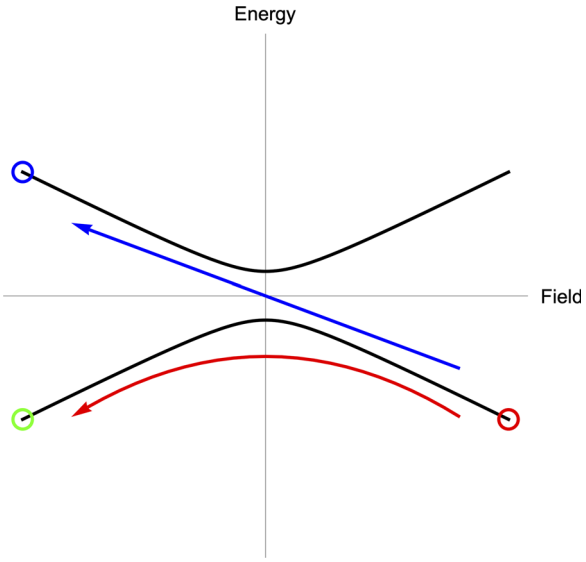

Fig. 5 Avoided crossing owing to a non-zero tunnelling gap. After magnetic polarisation (red circle), slow reversal of the magnetic field will lead to adiabatic passage and reversal of the magnetic moment *via* QTM (red arrow going to green circle). Fast reversal of the magnetic field can lead to a non-zero probability of a diabatic transition *via* Landau–Zenner tunnelling (blue arrow going to blue circle).

called non-adiabatic or diabatic passage. The probability of making such a transition is obtained from the Landau–Zenner tunnelling formula $p = \exp[-\pi\Delta^2/2\hbar\alpha]$, where Δ is the tunnelling gap and $\alpha = g_{\text{eff}}\mu_B \mathrm{d}B/\mathrm{d}t$ is the rate of change of the Zeeman energy of the pseudo-doublet.[91,94] Thus, how fast the field needs to be swept to suppress QTM is intimately related to the size of the tunnelling gap, and hence sweep-rate dependent demagnetisation experiments are one way to measure the tunnelling gap.[94,95] Alternatively put, the larger the tunnelling gap, the faster the QTM rate at zero magnetic field (though note we will not discuss the time-dependence of the spin dynamics directly here).

Therefore, for non-Kramers ions, the first requirement to observe SMM properties is slow QTM in the ground state, which translates to a very small splitting within the ground state pseudo-doublet (perhaps <1 cm^{-1}). If this condition is fulfilled, then we can consider what happens if a molecule is excited from one of the ground states to the first excited state by a phonon. If this excited state is non-degenerate, then it is non-magnetic and hence would not support an energy barrier to magnetic relaxation above it. That is, the molecule could simply emit a phonon and return to either one of the pseudo-doublet ground states with approximately 50 : 50 probability; thus, the energy of this excited state would be a good estimate for U_{eff}. If, on the other hand, the excited state is a pseudo-doublet, then we consider the tunnelling gap of the excited state. If it is larger than say >1 cm^{-1}, then QTM in that excited state will be fast and hence the magnetic moment can reverse and emit a phonon to relax to the ground state; the energy of the excited doublet will be a good estimate for U_{eff}. If, however, the tunnel gap is small, then QTM may be slow enough for the molecule to be excited by another phonon to a further excited state. So on, and so forth, we consider the tunnel splitting of each excited state to determine at point QTM will facilitate reversal of the magnetisation to determine U_{eff}.

Another consideration is the orientation of the largest principle *g*-value for each of the excited pseudo-doublets. Even if the tunnel splitting is small, if the orientation of the largest principle *g*-value is not collinear with that of the ground state, then this state will also permit reversal of the magnetisation. Consider the extreme case where the excited state *g*-value is perpendicular to that of the ground state, then if the molecule is excited into this state it has already re-oriented its magnetic moment into the plane, and so reversal back to the opposing ground state *via* emission of a phonon is facile. Experience suggests that angles differing by $>15^\circ$ are sufficient for that state to define the upper limit of U_{eff} (although see SI and Fig. S2 for discussion on this point).

7.2 Kramers ions

For a Kramers ion we are guaranteed at least a doubly-degenerate ground state, and hence there is no tunnel splitting to worry about. Thus, in principle, there should be no QTM for Kramers ions. However, experiments indicate this is not true. QTM can be facilitated by hyperfine coupling to nuclear spins[96,97] but more commonly by the presence of transverse magnetic fields. Consider a doublet with *g*-values of $g_x = g_y = 1$ and $g_z = 19$: application of a magnetic field in the *xy*-plane can split the state because g_x and g_y are non-zero (recall that the *g*-value gives the gradient of the state energy as a function of magnetic field). Thus, if there is a fixed magnetic field in the plane (which can arise from the dipolar magnetic field of neighbouring magnetic molecules), then when the external magnetic field along the *z*-axis goes to zero there is an avoided crossing just like for a non-Kramers ion (Fig. 5). Hence, the presence of transverse magnetic fields and non-zero transverse *g*-values permits QTM in Kramers ions by directly mixing the opposing projections of the ground state magnetic moment. [This is the reason many experiments are conducted on doped samples, replacing a large portion of the Ln^{III} ions with diamagnetic La^{III}, Lu^{III} or Y^{III}, to reduce the magnitude of the internal dipolar fields experienced at each paramagnetic Ln^{III} ion.] Thus, QTM efficiency in Kramers doublets is related to the magnitude of the transverse *g*-values as well as the strength of the local transverse magnetic field.

With this in mind, the same process described above for non-Kramers ions can be carried out to predict U_{eff}. Excited states sharing a common easy-axis magnetic anisotropy with small transverse *g*-values suggests that they will support an energy barrier to magnetic reversal, but the first doublet that is non-collinear with the ground state or has a non-negligible transverse *g*-value will likely facilitate QTM and hence define U_{eff}. Looking back on SA-CASSCF-SO calculations of 20 high-performance monometallic Dy^{III} SMMs performed by our group,[67,85,98–107] we find that excited state QTM appears to be favoured when the product of the average transverse *g*-value of an excited Kramers doublet ($g_T = (g_1 + g_2 + g_3 \sin\theta_3)/3$) and the angle between the maximal *g*-values of the ground and excited Kramers doublet (θ_3)

are greater than 20; *i.e.* QTM will generally occur when $g_T\theta_3 > 20$ (see SI, Fig. S2).

7.3 Quantification of QTM rates and prediction of U_{eff}

Beyond the hand-waving rules discussed above, it is common plot a figure of the energy barrier (*e.g.* Fig. 4a) simply from the properties of the eigenstates of the Hamiltonian. While the transition rates between states due to the spin–phonon coupling can be determined fully *ab initio*, it is quite costly (but it can be done and is becoming more routine, see ref. 88, 92, 108 and 109). A common approximation is to assume that the oscillations of the Hamiltonian caused by phonons may act like an oscillating magnetic field and hence that the transition rates can be approximated by the average of the square modulus of the three Cartesian magnetic moment operators:

$$\gamma_{kf} \approx \frac{1}{3}\sum_{\alpha\in x,y,z}\left|\langle\psi_f|g_J\hat{J}_\alpha|\psi_k\rangle\right|^2$$

From earlier you will see that the off-diagonal matrix elements of the $\hat{J}_\alpha$ operators will in generally be non-zero as these operators will not necessarily be diagonal in the eigenstate basis of the Hamiltonian. You will also see that using these operators implies the action of $\hat{J}_\pm$ operators, which can cause transitions between states differing by $\Delta m_J = \pm 1$ (this is the EPR selection rule); in situations where the eigenstates are not pure $|m_J\rangle$ states but rather mixtures thereof, these matrix elements are scaled by the squares of wavefunction coefficients of pairs of states differing by $\Delta m_J = \pm 1$. We have favoured an approach that uses these ''rates'' to propagate a fictional population starting in the ground state with negative magnetic moment ''over the barrier'',[110] representing a relaxation process over the predicted energy barrier U_{eff} (Fig. 4a). Keep in mind, however, that these ''rates'' are generated by assuming a magnetic perturbation and a uniform phonon density of states and so they are not realistic. Indeed, phonons modulate the entire Hamiltonian and oscillating crystal field terms $\hat{O}_k^q$ can give rise to transitions between states differing by $\Delta m_J = \pm q$, and the phonon density of states of molecular crystals is highly featured.[109,111–115]

The rates above provide a way of estimating which states might be connected by phonons, and similarly-qualitative metrics for estimating QTM rates have been suggested. One approach considers the average internal dipolar magnetic field as a parameter B_{dip}, and then calculate the QTM rate arising as:[116]

$$\tau_{QTM} = \frac{h\sqrt{g_x^2 + g_y^2 + g_z^2}}{\mu_B B_{dip}\sqrt{g_x^2 + g_y^2}}$$

A slightly more realistic approach is to take assume a Gaussian distribution of dipolar fields and calculate the rates in a similar fashion.[117] These calculations make a lot of assumptions and so they best used to obtain qualitative estimates, and while more specific methods are possible,[91] these require far more in-depth calculations.

8 Conclusions

In this article I have attempted to provide a step-by-step guide to de-mystify the process of setting up, running, and interpreting a SA-CASSCF-SO calculation for Ln^{III}-based SMMs. All-in-all, there is a lot that can be learned about potential SMM behaviour from a SA-CASSCF-SO calculation, including insights into the dynamic magnetic properties, even before launching into more advanced topics such as explicit relaxation rate calculations. The interested reader should be able to use this guide as a starting point for calculation of optical properties of Ln^{III} complexes, or paramagnetic nuclear magnetic resonance effects, but these topics usually require more elaborate active spaces and calculation of additional properties.

Conflicts of interest

There are no conflicts to declare.

Data availability

The example input and output files can be found at DOI: **https://doi.org/10.48420/30028195**.

Supplementary information (SI): Dieke diagram, annotated OpenMolcas input file for SA-CASSCF-SO calculation, *ab initio*-calculated crystal field parameters, empirical method for predicting U_{eff}. See DOI: **https://doi.org/10.1039/d5cs00493d**.

Acknowledgements

I would like to thank Prof. Eric McInnes, Dr Meagan Oakley, Dr Benjamin Atkinson, Dr Jakob Staab, Dr Gemma Gransbury, William Morrillo and Leander Held for assistance, comments and suggestions that greatly improved this article. I thank the ERC (ERC-2019-STG-851504), the Leverhulme Trust (RPG-2023-025), The University of Manchester and The Australian National University for funding.

Notes and references

1 R. Sessoli, D. Gatteschi, A. Caneschi and M. A. Novak, *Nature*, 1993, **365**, 141–143.
2 D. Gatteschi, R. Sessoli and J. Villain, *Molecular Nanomagnets*, Oxford University Press, 2006.
3 L. Thomas, F. Lionti, R. Ballou, D. Gatteschi, R. Sessoli and B. Barbara, *Nature*, 1996, **383**, 145–147.
4 J. R. Friedman, M. P. Sarachik, J. Tejada and R. Ziolo, *Phys. Rev. Lett.*, 1996, **76**, 3830–3833.
5 R. Bagai and G. Christou, *Chem. Soc. Rev.*, 2009, **38**, 1011–1026.
6 J. D. Rinehart and J. R. Long, *Chem. Sci.*, 2011, **2**, 2078–2085.
7 N. F. Chilton, *Annu. Rev. Mater. Res.*, 2022, **52**, 79–101.
8 J.-L. Liu, Y.-C. Chen and M.-L. Tong, *Chem. Soc. Rev.*, 2018, **47**, 2431–2453.
9 S.-D. Jiang, B.-W. Wang and S. Gao, in *Molecular Nanomagnets and Related Phenomena*, ed. S. Gao, Springer, Berlin Heidelberg, 2014, pp. 111–141.

10 C. V. Topping and S. J. Blundell, *J. Phys.: Condens. Matter*, 2019, **31**, 013001.
11 W. J. A. Blackmore, G. K. Gransbury, P. Evans, J. G. C. Kragskow, D. P. Mills and N. F. Chilton, *Phys. Chem. Chem. Phys.*, 2023, **25**, 16735–16744.
12 P.-H. Lin, T. J. Burchell, L. Ungur, L. F. Chibotaru, W. Wernsdorfer and M. Murugesu, *Angew. Chem., Int. Ed.*, 2009, **48**, 9489–9492.
13 Y.-N. Guo, G.-F. Xu, W. Wernsdorfer, L. Ungur, Y. Guo, J. Tang, H.-J. Zhang, L. F. Chibotaru and A. K. Powell, *J. Am. Chem. Soc.*, 2011, **133**, 11948–11951.
14 L. Ungur and L. F. Chibotaru, *Phys. Chem. Chem. Phys.*, 2011, **13**, 20086–20090.
15 R. J. Blagg, L. Ungur, F. Tuna, J. Speak, P. Comar, D. Collison, W. Wernsdorfer, E. J. L. McInnes, L. F. Chibotaru and R. E. P. Winpenny, *Nat. Chem.*, 2013, **5**, 673–678.
16 L. Ungur and L. F. Chibotaru, *Lanthanides and Actinides in Molecular Magnetism*, John Wiley & Sons, Ltd, 2015, pp. 153–184.
17 F. Aquilante, L. De Vico, N. Ferré, G. Ghigo, P. Malmqvist, P. Neogrády, T. B. Pedersen, M. Pitoňák, M. Reiher, B. O. Roos, L. Serrano-Andrés, M. Urban, V. Veryazov and R. Lindh, *J. Comput. Chem.*, 2010, **31**, 224–247.
18 F. Aquilante, J. Autschbach, R. K. Carlson, L. F. Chibotaru, M. G. Delcey, L. De Vico, I. Fdez. Galván, N. Ferré, L. M. Frutos, L. Gagliardi, M. Garavelli, A. Giussani, C. E. Hoyer, G. Li Manni, H. Lischka, D. Ma, P. Å. Malmqvist, T. Müller, A. Nenov, M. Olivucci, T. B. Pedersen, D. Peng, F. Plasser, B. Pritchard, M. Reiher, I. Rivalta, I. Schapiro, J. Segarra-Martí, M. Stenrup, D. G. Truhlar, L. Ungur, A. Valentini, S. Vancoillie, V. Veryazov, V. P. Vysotskiy, O. Weingart, F. Zapata and R. Lindh, *J. Comput. Chem.*, 2016, **37**, 506–541.
19 I. Fdez. Galván, M. Vacher, A. Alavi, C. Angeli, F. Aquilante, J. Autschbach, J. J. Bao, S. I. Bokarev, N. A. Bogdanov, R. K. Carlson, L. F. Chibotaru, J. Creutzberg, N. Dattani, M. G. Delcey, S. S. Dong, A. Dreuw, L. Freitag, L. M. Frutos, L. Gagliardi, F. Gendron, A. Giussani, L. González, G. Grell, M. Guo, C. E. Hoyer, M. Johansson, S. Keller, S. Knecht, G. Kovačević, E. Källman, G. Li Manni, M. Lundberg, Y. Ma, S. Mai, J. P. Malhado, P. Å. Malmqvist, P. Marquetand, S. A. Mewes, J. Norell, M. Olivucci, M. Oppel, Q. M. Phung, K. Pierloot, F. Plasser, M. Reiher, A. M. Sand, I. Schapiro, P. Sharma, C. J. Stein, L. K. Sørensen, D. G. Truhlar, M. Ugandi, L. Ungur, A. Valentini, S. Vancoillie, V. Veryazov, O. Weser, T. A. Wesołowski, P.-O. Widmark, S. Wouters, A. Zech, J. P. Zobel and R. Lindh, *J. Chem. Theory Comput.*, 2019, **15**, 5925–5964.
20 G. Li Manni, I. Fdez. Galván, A. Alavi, F. Aleotti, F. Aquilante, J. Autschbach, D. Avagliano, A. Baiardi, J. J. Bao, S. Battaglia, L. Birnoschi, A. Blanco-González, S. I. Bokarev, R. Broer, R. Cacciari, P. B. Calio, R. K. Carlson, R. Carvalho Couto, L. Cerdán, L. F. Chibotaru, N. F. Chilton, J. R. Church, I. Conti, S. Coriani, J. Cuéllar-Zuquin, R. E. Daoud, N. Dattani, P. Decleva, C. De Graaf, M. G. Delcey, L. De Vico, W. Dobrautz, S. S. Dong, R. Feng, N. Ferré, M. Filatov(Gulak), L. Gagliardi, M. Garavelli, L. González, Y. Guan, M. Guo, M. R. Hennefarth, M. R. Hermes, C. E. Hoyer, M. Huix-Rotllant, V. K. Jaiswal, A. Kaiser, D. S. Kaliakin, M. Khamesian, D. S. King, V. Kochetov, M. Krośnicki, A. A. Kumaar, E. D. Larsson, S. Lehtola, M.-B. Lepetit, H. Lischka, P. López Ríos, M. Lundberg, D. Ma, S. Mai, P. Marquetand, I. C. D. Merritt, F. Montorsi, M. Mörchen, A. Nenov, V. H. A. Nguyen, Y. Nishimoto, M. S. Oakley, M. Olivucci, M. Oppel, D. Padula, R. Pandharkar, Q. M. Phung, F. Plasser, G. Raggi, E. Rebolini, M. Reiher, I. Rivalta, D. Roca-Sanjuán, T. Romig, A. A. Safari, A. Sánchez-Mansilla, A. M. Sand, I. Schapiro, T. R. Scott, J. Segarra-Martí, F. Segatta, D.-C. Sergentu, P. Sharma, R. Shepard, Y. Shu, J. K. Staab, T. P. Straatsma, L. K. Sørensen, B. N. C. Tenorio, D. G. Truhlar, L. Ungur, M. Vacher, V. Veryazov, T. A. Voß, O. Weser, D. Wu, X. Yang, D. Yarkony, C. Zhou, J. P. Zobel and R. Lindh, *J. Chem. Theory Comput.*, 2023, **19**, 6933–6991.
21 F. Neese, *Wiley Interdiscip. Rev.: Comput. Mol. Sci.*, 2012, **2**, 73–78.
22 R. E. P. Winpenny and E. J. L. McInnes, *Molecular Materials*, John Wiley & Sons, 2010.
23 B. G. Wybourne, *Spectroscopic properties of rare earths*, Interscience Publishers, New York, 1965.
24 A. Abragam and B. Bleaney, *Electron Paramagnetic Resonance of Transition Ions*, Oxford University Press, 1970.
25 M. Blume, *Phys. Rev.*, 1964, **134**, A320–A327.
26 M. Dunn, *Trans. Faraday Soc.*, 1961, 1441–1444.
27 S. Ohmura, T. Kato, T. Oyamada, S. Koseki, H. Ohmura and H. Kono, *J. Phys. B: At., Mol. Opt. Phys.*, 2018, **51**, 034001.
28 A. J. Walisinghe and N. F. Chilton, *Dalton Trans.*, 2021, **50**, 14130–14138.
29 W. C. Martin, R. Zalubas and L. Hagan, *Atomic energy levels – the rare-earth elements: the spectra of lanthanum, cerium, praseodymium, neodymium, promethium, samarium, europium, gadolinium, terbium, dysprosium, holmium, erbium, thulium, ytterbium, and lutetitum*, National Bureau of Standards, Gaithersburg, MD, 1978.
30 **https://pypi.org/project/molcas-suite/**.
31 **https://pypi.org/project/angmom-suite/**.
32 K. W. H. Stevens, *Proc. Phys. Soc., London, Sect. A*, 1952, **65**, 209–215.
33 M. Hutchings, *Solid State Physics*, Elsevier, Amsterdam, 1964, vol. 16, pp. 227–273.
34 J. Mulak and Z. Gajek, *The Effective Crystal Field Potential*, Elsevier, 2000.
35 I. D. Ryabov, *J. Magn. Reson.*, 1999, **140**, 141–145.
36 I. Ryabov, *Appl. Magn. Reson.*, 2009, **35**, 481–494.
37 C. Gorller-Walrand and K. Binnemans, *Handbook on the Physics and Chemistry of Rare Earths*, Elsevier, 1996, vol. 23.
38 J. Sievers, *Z. Phys. B: Condens. Matter*, 1982, **45**, 289–296.
39 N. F. Chilton, D. Collison, E. J. L. McInnes, R. E. P. Winpenny and A. Soncini, *Nat. Commun.*, 2013, **4**, 2551.
40 J. J. Sakurai and S. F. Tuan, *Modern quantum mechanics*, Addison-Wesley Pub. Co, Reading, Mass, Rev. ed., 1994.
41 E. U. Condon and G. Shortley, *The Theory of Atomic Spectra*, Cambridge University Press, 1951.

42 *Computational Methods in Lanthanide and Actinide Chemistry: Dolg/Computational Methods in Lanthanide and Actinide Chemistry*, ed. M. Dolg, John Wiley & Sons Ltd, Chichester, UK, 2015.
43 J. Autschbach, *J. Chem. Phys.*, 2012, **136**, 150902.
44 W. T. Carnall, G. L. Goodman, K. Rajnak and R. S. Rana, *J. Chem. Phys.*, 1989, **90**, 3443–3457.
45 B. N. Figgis and M. A. Hitchman, *Ligand Field Theory and Its Applications*, Wiley-VCH, 1st edn, 1999.
46 M. Gerloch, *Magnetism and ligand-field analysis*, Cambridge University Press, Cambridge [Cambridgeshire]; New York, 1983.
47 J. S. Griffith, *The Theory of Transition-Metal Ions*, Cambridge University Press, 1961.
48 F. E. Mabbs and D. J. Machin, *Magnetism and Transition Metal Complexes*, Chapman and Hall, 1973.
49 N. M. Edelstein, P. G. Allen, J. J. Bucher, D. K. Shuh, C. D. Sofield, N. Kaltsoyannis, G. H. Maunder, M. R. Russo and A. Sella, *J. Am. Chem. Soc.*, 1996, **118**, 13115–13116.
50 A. Kerridge and N. Kaltsoyannis, *C. R. Chim.*, 2010, **13**, 853–859.
51 P. Siegbahn, A. Heiberg, B. Roos and B. Levy, *Phys. Scr.*, 1980, **21**, 323.
52 C. Kollmar, K. Sivalingam, B. Helmich-Paris, C. Angeli and F. Neese, *J. Comput. Chem.*, 2019, **40**, 1463–1470.
53 P.-O. Löwdin and H. Shull, *Phys. Rev.*, 1956, **101**, 1730–1739.
54 V. Veryazov, P. Å. Malmqvist and B. O. Roos, *Int. J. Quantum Chem.*, 2011, **111**, 3329–3338.
55 C. A. P. Goodwin, M. J. Giansiracusa, S. M. Greer, H. M. Nicholas, P. Evans, M. Vonci, S. Hill, N. F. Chilton and D. P. Mills, *Nat. Chem.*, 2021, **13**, 243–248.
56 **https://pypi.org/project/Pegamoid/**.
57 P.-Å. Malmqvist and B. O. Roos, *Chem. Phys. Lett.*, 1989, **155**, 189–194.
58 K. Andersson, P. Aake. Malmqvist, B. O. Roos, A. J. Sadlej and K. Wolinski, *J. Phys. Chem.*, 1990, **94**, 5483–5488.
59 C. Angeli, R. Cimiraglia, S. Evangelisti, T. Leininger and J.-P. Malrieu, *J. Chem. Phys.*, 2001, **114**, 10252–10264.
60 O. Kahn, *Molecular magnetism*, Wiley-VCH, New York, 1993.
61 R. Boča, *Theoretical Foundations of Molecular Magnetism*, Elsevier, 1999.
62 N. F. Chilton, PHI User Manual v2.1, 2015.
63 M. Vonci, K. Mason, E. R. Neil, D. S. Yufit, E. J. L. McInnes, D. Parker and N. F. Chilton, *Inorg. Chem.*, 2019, **58**, 5733–5745.
64 K. Qian, J. J. Baldoví, S.-D. Jiang, A. Gaita-Ariño, Y.-Q. Zhang, J. Overgaard, B.-W. Wang, E. Coronado and S. Gao, *Chem. Sci.*, 2015, **6**, 4587–4593.
65 Y.-S. Ding, W. J. A. Blackmore, Y.-Q. Zhai, M. J. Giansiracusa, D. Reta, I. Vitorica-Yrezabal, R. E. P. Winpenny, N. F. Chilton and Y.-Z. Zheng, *Inorg. Chem.*, 2022, **61**, 227–235.
66 C. A. Gould, K. R. McClain, D. Reta, J. G. C. Kragskow, D. A. Marchiori, E. Lachman, E.-S. Choi, J. G. Analytis, R. D. Britt, N. F. Chilton, B. G. Harvey and J. R. Long, *Science*, 2022, **375**, 198–202.
67 M. Gregson, N. F. Chilton, A.-M. Ariciu, F. Tuna, I. F. Crowe, W. Lewis, A. J. Blake, D. Collison, E. J. L. McInnes, R. E. P. Winpenny and S. T. Liddle, *Chem. Sci.*, 2016, **7**, 155–165.
68 H. Bolvin, *ChemPhysChem*, 2006, **7**, 1575–1589.
69 M. Gerloch and R. F. McMeeking, *J. Chem. Soc., Dalton Trans.*, 1975, 2443–2451.
70 L. Chibotaru, A. Ceulemans and H. Bolvin, *Phys. Rev. Lett.*, 2008, **101**, 033003.
71 L. F. Chibotaru and L. Ungur, *Phys. Rev. Lett.*, 2012, **109**, 246403.
72 **https://pypi.org/project/PyMolVis/**.
73 J. K. Staab, PhD thesis, The University of Manchester, 2024.
74 L. F. Chibotaru, in *Advances in Chemical Physics*, ed. S. A. Rice and A. R. Dinner, John Wiley & Sons, Inc., 2013, pp. 397–519.
75 L. F. Chibotaru and L. Ungur, *J. Chem. Phys.*, 2012, **137**, 064112.
76 L. Ungur and L. F. Chibotaru, *Chem. – Eur. J.*, 2017, **23**, 3708–3718.
77 D. M. King, P. A. Cleaves, A. J. Wooles, B. M. Gardner, N. F. Chilton, F. Tuna, W. Lewis, E. J. L. McInnes and S. T. Liddle, *Nat. Commun.*, 2016, **7**, 13773.
78 J. A. Seed, L. Birnoschi, E. Lu, F. Tuna, A. J. Wooles, N. F. Chilton and S. T. Liddle, *Chem*, 2021, **7**, 1666–1680.
79 B. R. Judd, *Operator Techniques in Atomic Spectroscopy*, Princeton University Press, 1998.
80 *Science*, 2022, **378**, eadf5804.
81 H. Kwon, K. R. McClain, J. G. C. Kragskow, J. K. Staab, M. Ozerov, K. R. Meihaus, B. G. Harvey, E. S. Choi, N. F. Chilton and J. R. Long, *J. Am. Chem. Soc.*, 2024, **146**, 18714–18721.
82 P. Zhang, R. Nabi, J. K. Staab, N. F. Chilton and S. Demir, *J. Am. Chem. Soc.*, 2023, **145**, 9152–9163.
83 J. Du, B. E. Atkinson, J. A. Seed, R. F. Sheppard, F. Tuna, A. J. Wooles, N. F. Chilton and S. T. Liddle, *Chem*, 2025, **11**, 102494.
84 P.-B. Jin, Q.-C. Luo, G. K. Gransbury, I. J. Vitorica-Yrezabal, T. Hajdu, I. Strashnov, E. J. L. McInnes, R. E. P. Winpenny, N. F. Chilton, D. P. Mills and Y.-Z. Zheng, *J. Am. Chem. Soc.*, 2023, **145**, 27993–28009.
85 C. A. P. Goodwin, F. Ortu, D. Reta, N. F. Chilton and D. P. Mills, *Nature*, 2017, **548**, 439–442.
86 S.-D. Jiang, B.-W. Wang, G. Su, Z.-M. Wang and S. Gao, *Angew. Chem., Int. Ed.*, 2010, **49**, 7448–7451.
87 G.-J. Chen, C.-Y. Gao, J.-L. Tian, J. Tang, W. Gu, X. Liu, S.-P. Yan, D.-Z. Liao and P. Cheng, *Dalton Trans.*, 2011, **40**, 5579–5583.
88 A. Lunghi, *Sci. Adv.*, 2022, **8**, eabn7880.
89 J. Villain, F. Hartman-Boutron, R. Sessoli and A. Rettori, *Europhys. Lett.*, 1994, **27**, 159–164.
90 J. Villain and A. Fort, *Eur. Phys. J. B*, 2000, **17**, 69–83.
91 A. Mattioni, J. K. Staab, W. J. A. Blackmore, D. Reta, J. Iles-Smith, A. Nazir and N. F. Chilton, *Nat. Commun.*, 2024, **15**, 485.
92 J. G. C. Kragskow, A. Mattioni, J. K. Staab, D. Reta, J. M. Skelton and N. F. Chilton, *Chem. Soc. Rev.*, 2023, **52**, 4567–4585.

93 A. Fort, A. Rettori, J. Villain, D. Gatteschi and R. Sessoli, *Phys. Rev. Lett.*, 1998, **80**, 612–615.
94 F. Troiani, C. Godfrin, S. Thiele, F. Balestro, W. Wernsdorfer, S. Klyatskaya, M. Ruben and M. Affronte, *Phys. Rev. Lett.*, 2017, **118**, 257701.
95 W. J. A. Blackmore, A. Mattioni, S. C. Corner, P. Evans, G. K. Gransbury, D. P. Mills and N. F. Chilton, *J. Phys. Chem. Lett.*, 2023, **14**, 2193–2200.
96 F. Pointillart, K. Bernot, S. Golhen, B. Le Guennic, T. Guizouarn, L. Ouahab and O. Cador, *Angew. Chem., Int. Ed.*, 2015, **54**, 1504–1507.
97 E. Moreno-Pineda, G. Taran, W. Wernsdorfer and M. Ruben, *Chem. Sci.*, 2019, **10**, 5138–5145.
98 T. Pugh, N. F. Chilton and R. A. Layfield, *Angew. Chem., Int. Ed.*, 2016, **55**, 11082–11085.
99 Y.-S. Ding, K.-X. Yu, D. Reta, F. Ortu, R. E. P. Winpenny, Y.-Z. Zheng and N. F. Chilton, *Nat. Commun.*, 2018, **9**, 3134.
100 P. Evans, D. Reta, G. F. S. Whitehead, N. F. Chilton and D. P. Mills, *J. Am. Chem. Soc.*, 2019, **141**, 19935–19940.
101 K.-X. Yu, J. G. C. Kragskow, Y.-S. Ding, Y.-Q. Zhai, D. Reta, N. F. Chilton and Y.-Z. Zheng, *Chem*, 2020, **6**, 1777–1793.
102 L. R. Thomas-Hargreaves, D. Hunger, M. Kern, A. J. Wooles, J. Van Slageren, N. F. Chilton and S. T. Liddle, *Chem. Commun.*, 2021, **57**, 733–736.
103 L. R. Thomas-Hargreaves, M. J. Giansiracusa, M. Gregson, E. Zanda, F. O'Donnell, A. J. Wooles, N. F. Chilton and S. T. Liddle, *Chem. Sci.*, 2021, **12**, 3911–3920.
104 A. H. Vincent, Y. L. Whyatt, N. F. Chilton and J. R. Long, *J. Am. Chem. Soc.*, 2023, **145**, 1572–1579.
105 G. K. Gransbury, S. C. Corner, J. G. C. Kragskow, P. Evans, H. M. Yeung, W. J. A. Blackmore, G. F. S. Whitehead, I. J. Vitorica-Yrezabal, M. S. Oakley, N. F. Chilton and D. P. Mills, *J. Am. Chem. Soc.*, 2023, **145**, 22814–22825.
106 S. C. Corner, G. K. Gransbury, I. J. Vitorica-Yrezabal, G. F. S. Whitehead, N. F. Chilton and D. P. Mills, *Inorg. Chem.*, 2024, **63**, 9552–9561.
107 S. C. Corner, W. J. A. Blackmore, G. K. Gransbury, A. Mattioni, G. F. S. Whitehead, N. F. Chilton and D. P. Mills, *Chem. Sci.*, 2025, **16**, 610–620.
108 M. Briganti, F. Santanni, L. Tesi, F. Totti, R. Sessoli and A. Lunghi, *J. Am. Chem. Soc.*, 2021, **143**, 13633–13645.
109 R. Nabi, J. K. Staab, A. Mattioni, J. G. C. Kragskow, D. Reta, J. M. Skelton and N. F. Chilton, *J. Am. Chem. Soc.*, 2023, **145**, 24558–24567.
110 N. F. Chilton, *Inorg. Chem.*, 2015, **54**, 2097–2099.
111 R. Nabi, B. E. Atkinson, J. K. Staab, J. M. Skelton and N. F. Chilton, *Chem. Commun.*, 2024, **60**, 13915–13918.
112 A. Lunghi, F. Totti, R. Sessoli and S. Sanvito, *Nat. Commun.*, 2017, **8**, 14620.
113 A. Albino, S. Benci, L. Tesi, M. Atzori, R. Torre, S. Sanvito, R. Sessoli and A. Lunghi, *Inorg. Chem.*, 2019, **58**, 10260–10268.
114 E. Garlatti, L. Tesi, A. Lunghi, M. Atzori, D. J. Voneshen, P. Santini, S. Sanvito, T. Guidi, R. Sessoli and S. Carretta, *Nat. Commun.*, 2020, **11**, 1751.
115 A. Chiesa, F. Cugini, R. Hussain, E. Macaluso, G. Allodi, E. Garlatti, M. Giansiracusa, C. A. P. Goodwin, F. Ortu, D. Reta, J. M. Skelton, T. Guidi, P. Santini, M. Solzi, R. De Renzi, D. P. Mills, N. F. Chilton and S. Carretta, *Phys. Rev. B*, 2020, **101**, 174402.
116 B. Yin and C.-C. Li, *Phys. Chem. Chem. Phys.*, 2020, **22**, 9923–9933.
117 D. Aravena, *J. Phys. Chem. Lett.*, 2018, **9**, 5327–5333.